

COAPEC Project - Balancing the Atlantic Heat and Freshwater Budgets, Report No. 1

**BALANCING THE SOC CLIMATOLOGY USING INVERSE ANALYSIS  
WITH SPATIALLY FIXED PARAMETER ADJUSTMENTS**

Jeremy P. Grist and Simon A. Josey

James Rennell Division

Southampton Oceanography Centre

Southampton, U.K.

January 2002

## ABSTRACT

Early results from a project which has the aim of obtaining a balanced version of the SOC climatology using linear inverse analysis techniques are discussed. In particular, we investigate whether a set of balanced fields can be obtained using spatially fixed analysis parameter adjustments which satisfies the requirements of a.) global heat budget closure; b.) consistency with hydrographic estimates of regionally averaged surface heat fluxes, and c.) agreement with independent research buoy measurements. Results of analyses obtained using two formulations of the inverse method with up to ten ocean heat transport constraints distributed throughout the Atlantic and North Pacific oceans are presented. The first formulation is an established technique which utilises the heat transport estimates directly as constraints. The second is a novel application in which pairs of heat transport estimates are used to derive area averaged heat fluxes which are then employed as constraints. The solutions obtained in each case are found to be sensitive to the choice of location of the heat transport estimates when only a small number (less than 5) of constraints are applied. Consequently, we have focused on solutions obtained with the full set of ten hydrographic constraints both with and without the additional requirement that the globally averaged net flux should equal zero. Without this requirement solutions are obtained which have a net heat loss to the atmosphere of between 5 and 7  $\text{Wm}^{-2}$ . In order to close the global heat budget exactly it is necessary to specify it as an additional constraint. However, in this case the solution obtained with the heat transport method is not acceptable according to the criterion of Isemer et al. (1989) which requires the magnitude of the parameter adjustments to be smaller than the assumed error range for each. This criterion is satisfied if the requirement of exact closure is relaxed such that the global net heat flux is constrained to be  $0 \pm 2 \text{ Wm}^{-2}$ . In the latter case, the inverse analysis adjustments to the different components of the heat flux are increases of 19 % to the latent heat flux, 7 % to the sensible heat flux, 9 % to the longwave flux and a reduction of 6 % to the shortwave flux. Comparison of the adjusted fluxes with measurements made by various WHOI research buoys confirm the suggestion of Josey et al. (1999) that spatially fixed parameter adjustments lead to poorer agreement with the buoys than was found to be the case with the original SOC fluxes. This result indicates that spatially dependent adjustments of the free parameters in the inverse analysis are necessary in order to obtain a solution which is satisfactory in the sense that it meets the three requirements listed above.

## 1. INTRODUCTION

In this report we present early results from a Coupled Ocean-Atmosphere Processes and European Climate (COAPEC) funded project which has the primary aim of producing a balanced set of ocean-atmosphere heat exchange fields using the existing Southampton Oceanography Centre (SOC) climatology as a basis. It is well recognised that ship based estimates of air-sea heat fluxes have thus far been unable to produce a balanced ocean heat budget. In particular, there is a global mean net heat gain by the ocean of  $30\text{Wm}^{-2}$  in the SOC climatology (Josey et al., 1999), which is similar in magnitude to that found in an earlier analysis of ship reports by da Silva et al. (1994). The primary difference between the SOC climatology and that of da Silva et al. (1994) is that corrections for various ship reporting biases were included at the level of individual reports for the first time in the SOC analysis. However, although these corrections resulted in regional adjustments to the monthly mean heat exchange fields of up to  $10\text{Wm}^{-2}$ , they did not have a significant impact on the global mean heat flux imbalance. Thus, the problem of producing a globally balanced set of heat fluxes remains to be resolved.

Our aim is to address this problem by using the method of inverse analysis (Isemer et al., 1989), with independent measures of the ocean heat transport as constraints, to produce a balanced version of the SOC climatology. We have the advantage over previous inverse analysis studies, most recently that of da Silva et al. (1994), that there has been a recent significant increase in the number of ocean heat transport estimates available for use as constraints, primarily as a result of the World Ocean Circulation experiment (WOCE). The work described here represents an early step in this process of producing a revised SOC climatology. Results are presented from various inverse method corrections of the SOC climatology that have utilised spatially fixed adjustments of the free parameters in the analysis. We will show that it is not possible to satisfy all of the constraints using such spatially fixed adjustments and suggest that spatially varying adjustments are therefore required to produce a fully consistent solution. The spatially fixed analyses have however still proved to be useful as they have allowed us to become familiar with the inverse method and examine various issues associated with the analysis. In addition, the solutions that we have obtained from the analyses are likely to prove useful in the short term given the pressing requirement of the COAPEC and wider research communities for a balanced set of fields for use in modelling and other studies. In the next phase of our research, we plan to make use of independent high quality measurements of the fluxes from research buoys at various locations as further constraints and to employ spatially dependent parameter adjustments in the analysis.

The present report is the first of a sequence that will describe the research carried out within this COAPEC project. Other reports currently in preparation will describe the results of parallel research into the effects of aerosol loading on the SOC estimates of the shortwave flux and comparisons of the SOC net heat fluxes with independent datasets obtained via the residual method (Trenberth et al., 2001). The structure of the report is as follows, in the next section we present a brief summary of the SOC climatology and the hydrographic constraints used in our analysis. In Section 3 the inverse analysis method is described in detail. The main results of the

various analyses that we have carried out are presented in Section 4. Finally, we summarise and discuss the implications of these results in Section 5.

## 2. PRIMARY DATASET AND CONSTRAINTS

The primary dataset for our analysis is the SOC climatology which was derived from ship reports in the Comprehensive Ocean - Atmosphere Dataset 1a (Woodruff et al., 1993), covering the period 1980-1993. Additional information regarding observing procedure was merged onto this dataset from the International List of Selected, Supplementary and Auxiliary Ships which is published annually by the World Meteorological Organisation (e.g. WMO, 1993). The method used for the production of the climatology is fully described in Josey et al. (1998). Results from an evaluation of the climatology using hydrographic and research buoy measurements are discussed in Josey et al. (1999). For our inverse analysis we have utilized the SOC climatological mean fields of the shortwave, longwave, latent and sensible heat fluxes.

The constraints on the inverse analysis employed for the present study comprise various hydrographic estimates of the ocean heat transport together with the requirement of global heat budget closure. The latter is expressed either as zero net heat transport across the boundary of the Southern Ocean with Antarctica or as zero global mean net heat flux. The different heat transport estimates together with the source of each are listed in Table 1, each estimate has been given a constraint number for ease of reference. Note that an error estimate has been listed for each of the heat transport values used as constraints. These error estimates have been taken from the source reference relevant to each section.

The difference in heat transport estimates for neighbouring sections can be simply used to determine the area averaged net surface flux for the region which they span. We have also used these area averaged fluxes as constraints in an alternative formulation of the inverse problem. Details of the regions used are listed in Table 2, together with the area averaged values for each of the heat flux components and the net heat flux determined from the original SOC climatology. Each region has been given a label for reference purposes, the locations of the various hydrographic sections and regions are shown on Fig. 1. The area averaged net heat flux, determined from the bounding section estimates of the heat transport, and the difference between this value and the SOC estimate for each region are also listed in Table 2. Note that the sign convention is for positive heat fluxes to represent heat gain by the ocean. The SOC estimates are seen to typically underestimate the heat loss (or overestimate the heat gain depending on region considered) relative to the hydrographic values by between 20 and 50  $\text{Wm}^{-2}$  with the strongest bias occurring in the AT67 region of the North Atlantic which contains the Gulf Stream.

## 3. THE INVERSE METHOD

In this section we present the details of the inverse method. We begin by considering the simple case of a single constraint before generalising to multiple constraints. The problem may be formulated both in terms of area averaged heat flux and heat transport constraints and we consider both cases. Throughout this report we refer to them as the area averaged flux approach

and the heat transport approach respectively. Our formulation of the problem is based on that of Isemer et al. (1989) who in turn drew on the work of Menke (1984) to which the interested reader is referred for a detailed discussion of the principles of the method.

### 3.1. Formulation of Method

#### 3.1.1 Single Constraint.

Consider first the inverse method with a single constraint which might be that the heat transport at a given latitude or the area averaged heat flux for a particular region takes a certain value. We write down the equations for the case of an area averaged heat flux constraint,  $\hat{Q}_N$ , but note that they may be simply modified for heat transport as discussed later. Estimates of the net heat flux and its components prior to carrying out the inverse analysis adjustment are denoted by the superscript \*, and referred to here as the *original* estimates.

For the purposes of the analysis we introduce a number,  $m$ , of adjustable parameters,  $p_1, \dots, p_m$ , into the bulk formulae used to estimate each of the four heat flux components (see Josey et al., 1998 for details of the formulae). These parameters may appear as coefficients on individual variables, for example specific humidity, within each equation or more simply as coefficients on the full formula for each component. The initial values for these parameters are set equal to 1 and are also denoted by the superscript \*. The original area averaged net heat flux,  $\langle Q_N^* \rangle$ , for a particular region bounded by latitudes  $\varphi_1$  and  $\varphi_2$  may then be written as a function of the bounding latitudes and the free parameters,

$$\langle Q_N^* \rangle = f(\varphi_1, \varphi_2, p_1^*, \dots, p_m^*) \quad (1a)$$

$$= \frac{1}{S} \iint_{\text{Region}} Q_{Nxy}^*(p_1^*, \dots, p_m^*) dS \quad (1b)$$

where  $dS$  is an area element of the region considered, which has total area  $S$ , and  $Q_{Nxy}^*$  is the original net heat flux estimate for a given  $1^\circ \times 1^\circ$  cell. Note that for convenience we drop the brackets denoting an average in what follows, thus  $Q_N^*$  and  $\hat{Q}_N$  are taken to implicitly refer to area averaged values. The aim of the inverse method is to modify the values of the free parameters such that an *adjusted* estimate of the net heat flux may be obtained which equals the constraint  $\hat{Q}_N$ . Thus, new values  $\hat{p}_1, \dots, \hat{p}_m$  of the parameters are sought which satisfy the equation,

$$\hat{Q}_N = f(\varphi_1, \varphi_2, \hat{p}_1, \dots, \hat{p}_m) \quad (2)$$

Note that  $\hat{Q}_N$  is obtained from the difference of the hydrographic estimates of the heat transport at the bounding latitudes,  $\hat{H}_1$  and  $\hat{H}_2$ , as follows,

$$\hat{Q}_N = (\hat{H}_1 - \hat{H}_2)/S \quad (3)$$

and that each of the hydrographic estimates has an associated observational error,  $\sigma_1$  and  $\sigma_2$ , which we combine in quadrature to obtain the following error estimate on  $\hat{Q}_N$ ,

$$\hat{\sigma} = (\sigma_1^2 + \sigma_2^2)^{1/2}/S \quad (4)$$

In order to obtain values for  $\hat{p}_1, \dots, \hat{p}_m$  which satisfy (2), we first note that for sufficiently small parameter changes, the adjusted net heat flux can be expressed as a linear expansion of the original estimate,

$$\hat{Q}_N = Q_N^* + \sum_{i=1,m} A_i (\hat{p}_i - p_i^*) = Q_N^* + \sum_{i=1,m} A_i x_i \quad (5)$$

Where  $A_i = \partial Q_N^* / \partial p_i^*$  are the sensitivities of the original net heat flux estimate to changes in the various parameters and for convenience we have defined the adjustment to each individual parameter to be  $x_i = \hat{p}_i - p_i^*$ . Note that  $x_i$  is also occasionally referred to as  $dp_i$  in the literature and we have occasionally made use of this alternative notation later in the report. Rearranging (5) we have the following linear constraint on the parameter adjustments,

$$\sum_{i=1,m} A_i x_i = \hat{Q}_N - Q_N^* \quad (6)$$

For the case where the heat flux constraint is assumed to have zero error, equation (6) is solved subject to the least squares condition,

$$\sum_{i=1,m} (x_i^2 / e_i^2) = \text{minimum} \quad (7)$$

where the  $e_i$  are the standard deviations of the  $p_i^*$  which are assumed to be independent, normally distributed random variables. The least squares condition follows from a Maximum Likelihood principle given this assumption (Isemer et al., 1989). Using the method of Lagrange multipliers (e.g. Menke, 1984) the following solution for the adjustment to the  $i^{\text{th}}$  parameter can then be found:

$$x_i = (\hat{Q}_N - Q_N^*) e_i^2 A_i / \sigma^{*2} \quad (8)$$

where the weighting factor,

$$\sigma^{*2} = \sum_{i=1,m} e_i^2 A_i^2 \quad (9)$$

Note that for convenience, the individual parameter adjustments are often combined to form the solution vector  $\mathbf{x} = (x_1, \dots, x_m)$ .

Typically the constraint is not exact as assumed above and instead has a non-zero observational error  $\hat{\sigma}$ . In this case, the least squares condition (7) becomes

$$\sum_{i=1,m} x_i^2 / e_i^2 + (\hat{Q}_N - Q_N^*)^2 / \hat{\sigma}^2 = \text{minimum} \quad (10)$$

and the solution is modified as follows,

$$x_i = (\hat{Q}_N - Q_N^*) e_i^2 A_i / (\sigma^{*2} + \hat{\sigma}^2) \quad (11)$$

We present the extension of this method to the case of multiple constraints in the next section but before doing so we briefly discuss the choice of adjustment parameters employed for the present study. As noted above the adjustment parameters may appear as coefficients on individual variables within the bulk formulae or more simply as coefficients on the full formula for each

component. For the analyses presented here we have focused on the latter case defining the parameters as follows,

$$Q_N^* = p_E^* Q_E^* + p_H^* Q_H^* + p_S^* Q_S^* + p_L^* Q_L^* \quad (12)$$

where  $Q_E^*$ , is the area averaged latent heat flux;  $Q_H^*$ , the sensible heat flux;  $Q_S^*$ , shortwave radiation and  $Q_L^*$ , longwave radiation. Note that the subscripts E, H, L and S will be used more generally to specify the values of variables, such as the parameter adjustments, that are associated with each of the flux components. Differentiating  $Q_N^*$  with respect to  $p_i^*$  then yields:

$$A_E = Q_E^*, A_H = Q_H^*, A_S = Q_S^*, A_L = Q_L^* \quad (13)$$

i.e. the sensitivity terms are simply the original estimates of each flux component.

The selection of an appropriate error range for each parameter is the most difficult part of the analysis. In subsequent studies we plan to include spatially dependent error fields for the different parameters based on the results of separate investigations. In particular, work carried out thus far on the effects that neglect of aerosol loading have had on the original SOC shortwave flux estimates (Grist and Josey, 2002) has allowed us to quantify the contribution to the shortwave error field due to this process. At present we are, however, concerned primarily with exploring the effects of applying different levels of constraints on the outcome of inverse analyses with spatially fixed parameter adjustments. With this in mind have focused on the following 3 scenarios for the parameter errors:

Scenario 1:  $e_E = e_H = e_S = e_L = 0.2$

Scenario 2:  $e_E = e_H = 0.2$  and  $e_S = e_L = 0.1$

Scenario 3:  $e_E = e_H = 0.1$  and  $e_S = e_L = 0.2$

The various scenarios allow for 10-20% error in the original estimates of each flux component and thus are not unrealistic. Regarding the acceptability of different solutions to the analysis, we have adopted the approach of Isemer et al (1989) who discuss the difficulties that arise with formal confidence tests and suggest that the solutions be deemed acceptable if they satisfy the simple consistency check that  $|x_i| < e_i$  for all  $i$ .

### 3.1.2 Multiple Constraints

The method described above may be simply extended (Isemer et al., 1989) to be used with  $n > 1$  constraints,  $\hat{Q}_N(j)$  for  $j = 1, \dots, n$ , in which case the solution is,

$$\mathbf{x} = W_e^{-1} A^T [A W_e^{-1} A^T + W_\sigma^{-1}]^{-1} \mathbf{h} \quad (14)$$

where  $W_e = \text{diag}(e_1^{-2}, \dots, e_m^{-2})$  is a square matrix containing the reciprocals of the parameter errors squared;  $A$  is an  $n$  by  $m$  matrix, with elements

$$A_{ji} = \partial Q_{N(j)}^* / \partial p_i^* \quad (15)$$

;  $W_\sigma = \text{diag}(\sigma_1^{-2}, \dots, \sigma_n^{-2})$  is the weighting matrix of the constraint errors and  $\mathbf{h}$  is a vector of dimension  $n$  containing the difference ( $\hat{Q}_N(j) - Q_N^*(j)$ ) between the constraint and the original estimate for each of the  $n$  constraints.

### 3.2 Modification of Method for Heat Transport Constraints

The method presented in Sec 3.1 holds with slight modifications for the case where hydrographic estimates of the ocean heat transport are used directly as constraints rather than indirectly to formulate area averaged heat fluxes. In this case the original climatological estimate of the heat transport,  $H_y^*$ , at latitude  $y$  is obtained by integrating the net heat flux southwards across successive latitude bands from a reference latitude  $y_0$  which has a known value of the heat transport,  $H_0$ , from hydrography,

$$H_y^* = H_0 - \int_y^{y_0} \int_{x_1}^{x_2} Q_{Nxy}^* dx dy \quad (16)$$

where  $x_1$  and  $x_2$  are the longitude limits at the western and eastern continental boundaries respectively of a given latitude band. In this study, we have used values for  $H_0$  of 0.1 PW at  $65^\circ\text{N}$  in the Atlantic and 0.002 PW at  $66^\circ\text{N}$  in the Pacific (Aagaard and Greisman 1975) and assumed that the errors on these estimates are sufficiently small that they can be treated as exact measurements.

As before we seek parameter adjustments, such that the adjusted ocean heat transport at latitude  $y$  is equal to the hydrographic value being used as a constraint,  $\hat{H}_y$ . For the case where the parameters are simple scaling coefficients for each of the bulk formulae we therefore seek adjustments which satisfy the equation,

$$\hat{H}_y = H_0 - \int \int (\hat{p}_E Q_{Exy}^* + \hat{p}_H Q_{Hxy}^* + \hat{p}_S Q_{Sxy}^* + \hat{p}_L Q_{Lxy}^*) dx dy \quad (17)$$

The solution to the problem is still given by (14) although there are some minor changes to the matrix elements. Specifically, the elements of  $A$  are now

$$A_{ji} = \partial H_j^* / \partial p_i^* \quad (18)$$

while the elements of  $W_0$  are now the errors of the hydrographic heat transport estimates and the vector  $\mathbf{h}$  contains the difference between the hydrographic measurement and the original SOC estimate of the heat transport for each latitude at which there is a constraint. The elements of  $W_e$  remain unchanged. Substituting (16) into (18), we find that for the case where the adjustable parameters are as defined in (12) the elements of the sensitivity matrix are as follows,

$$\begin{aligned} A_{jE} &= - \int \int Q_{Exy}^* dx dy, & A_{jH} &= - \int \int Q_{Hxy}^* dx dy, \\ A_{jS} &= - \int \int Q_{Sxy}^* dx dy, & A_{jL} &= - \int \int Q_{Lxy}^* dx dy \end{aligned} \quad (19)$$

Equivalently,

$$A_{jE} = -Q_E^* S_k, \quad A_{jH} = -Q_H^* S_k, \quad A_{jS} = -Q_S^* S_k, \quad A_{jL} = -Q_L^* S_k \quad (20)$$

where  $S_k$  is the area between the reference latitude  $y_0$  and the section being considered. With these minor changes to the matrix elements, the solution of the inverse problem using heat transport constraints directly is given by (14).

For the results presented in Section 4, the various inverse problem solutions have been determined by evaluating (14) using the matrix inversion facility within the Matlab software package. In order to test the program used to do this, the solutions have been evaluated by hand for an idealised case in which two constraints are applied for both the area averaged heat flux and heat transport approaches. The relevant equations are presented in Appendix 1. In addition to providing confirmation that our computational method is correct they demonstrate that although the solutions obtained with the area averaged heat flux and heat transport approaches are similar they are not identical.

Finally, in this section we note a potential problem with the area averaged heat flux approach that has been brought to our attention during this study. In order to obtain the least squares condition (10) by application of the maximum likelihood principle, the following three conditions are assumed to be met (Menke, 1984; da Silva et al., 1994) :

- 1) The bulk formula parameter errors  $e_i$  are normally distributed and uncorrelated.
- 2) The constraint errors  $\sigma_j$  are normally distributed and uncorrelated.
- 3) The bulk formula parameter errors and constraint errors are not correlated with each other.

As a consequence, care has to be taken when using area averaged fluxes as condition (2) is broken if adjacent regions are included in the calculation (Ganachaud, personal comm.). This problem arises because the hydrographic measurement error for the latitude circle common to both of the adjacent regions is used in the calculation of  $\sigma_j$  for each region and consequently the  $\sigma_j$  are not uncorrelated. The problem may be avoided by using only the ocean heat transport approach for inverse calculations involving adjacent regions. In practice, the results presented in Appendix 1 and in the following Section demonstrate that despite condition (2) being broken in the area averaged flux approach the resulting solutions are physically reasonable and tend to be similar to those obtained with the heat transport method.

## 4. RESULTS

In this section we present the results of our inverse analysis calculations using spatially fixed adjustments of the free parameters. Various combinations of constraints have been considered, we begin with the simple scenario of the single constraint of global heat budget closure before examining multiple constraint analyses.

### 4.1 Single Constraint Analysis

For illustrative purposes we consider first the results of a simple analysis with the single constraint of global heat budget closure. In this case the solution to the problem is provided by (8) which indicates that the magnitude of the adjustment for each parameter is proportional to the sensitivity of the constraint to the parameter and the parameter error squared. In this case the sensitivity term is simply the original magnitude of the flux component corresponding to each of the parameters. Three different combinations of parameter errors have been considered as described in Section 3.1.1 and the results for each are listed in Tables 3 to 5.

The results for Scenario 1, in which each of the parameter errors,  $e_i$ , are assumed to be the same and equal to 0.2, illustrate the simple proportionality of the  $x_i$  terms in the solution to the original magnitude of each flux component. Note that the same result would have been obtained if we had assumed instead that  $e_i=0.1$  for all  $i$ , and indeed for all cases where the parameter errors are assumed to be equal, irrespective of the particular numerical value assumed for the error. This result arises because the  $e_i$  terms in the denominator and numerator of (8) cancel out when they are the same for all parameters.

The results for the other two scenarios illustrate the dependence of the solution on differences between the  $e_i$  when they do not all take the same value, the fractional adjustments increasing in magnitude with the assumed error for each. For example, the latent heat and shortwave adjustments are 16% and -8% respectively when a 20% error is assumed for the former and a 10% error for the latter. When this error assumption is reversed (i.e. 10% error on the latent and 20% for the shortwave) the magnitude of the adjustment to the latent heat flux falls to 2% while that for the shortwave increases to -15%. Note that the adjustments for Scenario 2 are similar to those obtained in the inverse analysis of da Silva et al (1994) - see their Table 11 -who assumed a more complicated form for the dependence of the bulk formula estimates on the adjustable parameters but made similar assumptions about the error range for each. Finally, note also that for all of the adjustments the condition that  $|x_i| < e_i$  is met, so the solutions are deemed acceptable according to the criterion of Isemer et al. (1989).

#### 4.2 Multiple Constraint Analyses

We now consider results from a number of inverse analyses carried out with varying combinations of multiple constraints. Analyses have been carried out with both the heat transport and area averaged flux approaches. We focus on results obtained from analyses in which an increasing number of the constraints listed in Tables 1 and 2 have been applied as described below. Various other combinations of constraints have also been considered and we refer to the results of these other analyses briefly where appropriate. In particular, all of the results presented here have been obtained with Scenario 1 for the parameter errors. Similar results regarding the effects of including differing sequences of constraints have also been obtained with the other two scenarios.

First, we consider results obtained under the following four cases:

- A) heat transport approach, no requirement of global heat budget closure,
- B) area averaged flux approach, no requirement of global heat budget closure,
- C) heat transport approach together with the requirement of exact global heat budget closure (i.e. that the globally averaged net heat flux equals zero),
- D) area averaged flux approach together with the requirement of exact global heat budget closure.

In each case we have applied the various constraints summarised in Tables 1 and 2 in sequential order. For example, for case A we have first carried out an analysis using constraint 1 in Table 1 (referred to as the 1 constraint solution), then an analysis with constraints 1 and 2 (referred to as

the 2 constraint solution), then with constraints 1, 2 and 3 (the 3 constraint solution), and so on. Constraints from Table 1 have been used for cases A and C, while constraints from Table 2 have been used for cases B and D. The analysis solutions are detailed in Tables 6 to 9 and shown graphically in Figs. 2a-b. Results from cases A and B are discussed in the next section and from cases C and D in Section 4.2.2.

#### 4.2.1 Analysis Solutions Without the Requirement of Global Heat Budget Closure

Consider first cases A and B for which the analysis solutions are summarised in Fig. 2a. The required parameter adjustments for each component are similar for both the surface flux and heat transport approaches despite the earlier caution that the area averaged flux method breaks the condition that the errors on the constraints should be independent when adjacent regions are used in the calculation.

In both case, the size of the parameter adjustments is seen to depend to some extent on the combination of constraints chosen. In particular, as the number of constraints increases beyond 4 - i.e. as values from the South Atlantic and the Pacific are included in the calculation - the magnitude of the fractional shortwave reduction,  $dp_s$ , falls sharply from about 0.18 to 0.11; at the same time there are small increases in the adjustments of the three heat loss terms. In addition, a sharp transition in the parameter values occurs between the one and two constraint solutions. This variation reflects the change in impact on the analysis of the region containing the Gulf Stream which is the second constraint to be applied. The Gulf Stream region (AT67) has been previously shown to exhibit the strongest biases, of order  $50 \text{ Wm}^{-2}$ , in the SOC fluxes when compared with hydrography (Josey et al., 1999), see also the final column of Table 2. Consequently, when the Gulf Stream region is included and the number of constraints is small the inverse analysis produces a large adjustment to the fluxes in order to redress the SOC-hydrography flux imbalance. For the analyses discussed here this is achieved primarily by a strong reduction in the shortwave flux. As more regions, which have smaller imbalances, are included the relative weight of the Gulf Stream bias in the analysis is reduced and the shortwave adjustment becomes smaller. We note that separate analyses, not discussed in detail here, in which the Tropical constraints are retained but the North Atlantic regions are excluded show smaller reductions to the shortwave than those obtained with the Gulf Stream region included. This is due to the original flux estimates having a reduced bias with respect to hydrography in the Tropics compared to the Gulf Stream region which necessitates only a small reduction to the shortwave in the inverse analysis.

The impact of the adjustments on the area averaged net heat fluxes for the various regions considered for cases A and B are detailed in Tables 10 and 11. For each region we have tabulated the difference between the adjusted net flux and the flux that the hydrography implies. The bottom row indicates how close the global ocean net heat flux is to being balanced. We note that the large parameter adjustments arising as a result of the inclusion of the Gulf Stream region in the 2 constraint case give rise to a strong global average heat loss of  $-17.3$  ( $-16.1$ )  $\text{Wm}^{-2}$  for the heat transport (surface flux) approach. As additional constraints are included, the reduction in the magnitude of the shortwave adjustment noted earlier leads to globally averaged values which are closer to zero.

When all ten constraints are applied the area averaged adjusted fluxes for each region are typically within  $\pm 20 \text{ Wm}^{-2}$  of the hydrographic values in both cases A and B whereas prior to the

adjustment they tended to have positive biases of 20 - 50  $\text{Wm}^{-2}$ , see Table 2 final column. We regard this change as an improvement in that there is no longer a strong positive bias but it remains the case that there are regional biases of  $\pm 20 \text{ Wm}^{-2}$  in the fluxes after the inverse calculation which points to the need for spatially varying parameter adjustments in subsequent analyses. In addition, the results indicate that the analysis is sensitive to the choice of constraints, in that use of values for the North Atlantic alone leads to large parameter adjustments and a strong negative bias in the globally averaged flux. Thus, if an improved set of global fields is required it is probably best to focus on solutions in which as wide a range of constraints as possible have been used in order to avoid particular regions dominating.

We refer to the solutions obtained using all 10 constraints in cases A and B as solutions  $A_{10}$  and  $B_{10}$  respectively. For solution  $A_{10}$  ( $B_{10}$ ) the required adjustments to the heat flux components are 6% (4%) for sensible heat, 15% (12%) for latent heat, 9% (8%) for longwave and -9% (-12%) for shortwave. Consideration of the globally averaged flux (Tables 10 and 11) indicates that of the two solutions, the heat transport one ( $A_{10}$ ) is to be preferred on the grounds of being closest to the requirement of closure of the global heat budget which has not been included in these analyses. The globally averaged flux for solution  $A_{10}$  is  $-5.0 \text{ Wm}^{-2}$ , compared with  $-6.7 \text{ Wm}^{-2}$  for  $B_{10}$ .

Maps of the difference between the adjusted and original heat flux component fields for solutions  $A_{10}$  and  $B_{10}$  are shown in Figs. 3 and 4. For completeness we have shown in both cases the difference field for each individual component but note that these are simply scaled versions of the original fields where the scaling factor is the appropriate parameter adjustment. Thus, for example, the latent heat flux difference field shows stronger adjustments in Fig. 4 than Fig. 3 because  $dp_E$  is somewhat larger (0.15) for solution  $A_{10}$  than for  $B_{10}$  (0.12). The combined effect of the changes to the different components on the adjustment to the net heat flux field is shown in Figs. 5a-b. The change in the net heat flux field is dominated by the adjustments to the shortwave and latent heat flux fields in the Tropics and mid-latitudes. It is notable that at high latitudes in both hemispheres the adjustment to the fluxes is small and in part this is a consequence of the fact that the inverse analysis as formulated here cannot produce large changes in regions where the original flux estimates are close to zero. The greatest difference between the two solutions without heat budget closure occurs in the Tropics reflecting the larger reduction in the shortwave flux field in the inverse analysis for solution  $B_{10}$  relative to solution  $A_{10}$ .

#### 4.2.2 Analysis Solutions with the Requirement of Global Heat Budget Closure

Results obtained with the requirement of heat budget closure included explicitly as one of the constraints on the analysis are considered next. We discuss in detail results from the problem where heat budget closure was required to be exact, i.e. cases C and D described earlier. We have also considered the effects of relaxing this assumption and allowing a small  $2 \text{ Wm}^{-2}$  error on the requirement that the globally averaged heat flux equals zero and briefly discuss the solutions obtained under this condition at the end of this section.

The solutions with the requirement of exact closure of the ocean heat budget are summarised in Fig. 2b and detailed in Tables 8-9 and 12-13. The main effect of this additional requirement in both cases is to reduce the impact of the Gulf Stream region such that the magnitude of the shortwave parameter adjustment does not increase strongly when constraint 2 is

applied. This is to be expected given that the globally averaged heat flux is forced to be exactly zero as large adjustments of the parameters to meet the Gulf Stream constraint, which would at the same time cause the globally averaged flux to become significantly negative, are not allowed by the analysis.

It is noticeable that in the heat flux case the adjustments retain similar magnitudes as additional constraints are included. However, in the heat transport case there is a noticeable shift towards stronger latent heat and weaker shortwave parameter adjustments when the South Atlantic and Pacific constraints are applied in addition to those in the North Atlantic. In particular the adjustments for 5 or more constraints do not satisfy the acceptability condition of Isemer et al. (1989) because  $dp_E$  is greater than the value of 0.2 taken for  $e_E$ , although only by a relatively small amount. We refer to the solutions obtained using all 10 constraints in cases C and D as solutions  $C_{10}$  and  $D_{10}$  respectively. The adjustments required for solution  $C_{10}$  ( $D_{10}$ ) are 9% (5%) for sensible heat, 25% (12%) for latent heat, 8% (9%) for longwave and -2% (-8%) for shortwave. The resulting spatial variation of these adjustments is shown in Figs. 6 and 7 and their impact on the net heat flux in Figs. 5c-d. The fields for solution  $C_{10}$  in Fig. 6 clearly illustrate that virtually all of the adjustment required to balance the global heat budget and achieve regional agreement with hydrography is being carried out by the strong reduction in the latent heat flux. The corresponding fields for solution  $D_{10}$  show a more even partition in the adjustment between the shortwave and latent heat fields. As a consequence of these differences, the net heat flux adjustments in Fig. 5 show stronger reductions over the western boundary current regions in solution  $C_{10}$  relative to solution  $D_{10}$ .

Further analyses have shown that if the requirement of exact closure of the global ocean heat budget is relaxed, such that a  $2 \text{ Wm}^{-2}$  error is permitted ( a scenario which we refer to as case E), a solution with all 10 constraints ( $E_{10}$ ) can be found which satisfies the Isemer et al. (1989) criterion. The results for this case are summarised in Fig. 1c and tabulated in detail in Tables 14 and 15. The parameter adjustments for solution  $E_{10}$  are a 19% increase in latent heat, 7% increase in sensible heat, 9% increase in longwave and a 6% decrease in shortwave. The adjustments to the component fields are plotted in Fig. 8 and the adjustment to the net flux field in Fig. 5e. These show that the effect of the inverse analysis for solution  $E_{10}$  is to produce a set of adjustments to the fluxes that are typically intermediate in magnitude between solutions  $C_{10}$  and  $D_{10}$  discussed above.

The impact on the area averaged fluxes of all three series of solutions discussed above are similar to those found in Sec. 4.2.1 in that agreement with hydrography to within  $\pm 20 \text{ Wm}^{-2}$  is typically found. The level of agreement for solution  $E_{10}$  is compared graphically in Fig. 9 with that obtained with the original SOC fluxes. The figure shows that although there are imbalances of up to  $20 \text{ Wm}^{-2}$  following the analysis, no particular region stands out as being strongly biased. As regards the globally averaged net heat flux, for the exactly constrained cases the value is zero by definition. For solution  $E_{10}$  the global average net heat flux equals  $-2.3 \text{ Wm}^{-2}$ .

Summarising the various 10 constraint solutions, it is evident that although the area averaged flux solutions  $B_{10}$  and  $D_{10}$  should be discarded given the risk of error correlation they do not appear to have lead to physically unrealistic results. Solution  $C_{10}$  (heat transport approach with global closure) is technically unacceptable because the required latent heat flux adjustment is too large in the sense that the Isemer et al. (1989) criterion is not satisfied. In addition it appears to be physically the least reasonable of the solutions given that there are very strong increases in the latent heat flux and only a minor reduction in the shortwave. The two remaining heat transport

approach solutions,  $A_{10}$  and  $E_{10}$ , are potentially more useful as they are not affected by possible correlation of errors and do satisfy the Isemer et al. (1989) criterion. For solution  $A_{10}$  the global heat budget is closed to within  $5 \text{ Wm}^{-2}$  and for solution  $E_{10}$  it is closed to within  $2.5 \text{ Wm}^{-2}$ . On this basis we suggest that of the five solutions considered  $E_{10}$  is to be preferred.

Finally, we briefly consider the implied ocean heat transport for each of the five main solutions that we have considered. The transport in the Atlantic, Pacific and combined Global Oceans has been calculated by integrating the net heat flux southwards with respect to the northern reference values listed in Table 1. The results are shown on Fig. 10 together with the heat transport obtained with the original SOC fluxes and the various hydrographic reference values. As has been noted before, the global mean net heat flux imbalance of  $30 \text{ Wm}^{-2}$  in the original fields leads to a rapid divergence of the ocean heat transport from the hydrographic values in all three basins. The five solutions share broadly similar transport curves and are in reasonable agreement with the majority of the hydrographic estimates as is to be expected given that these were used as constraints on the analysis. The impact of the small negative values for the globally averaged heat flux in solutions  $A_{10}$ ,  $B_{10}$  and  $E_{10}$  is evident as an apparent northwards transport across the southern boundary in the third panel of the figure. For solutions  $A_{10}$  and  $B_{10}$  the magnitude of the southern boundary transports are uncomfortably large, i.e. of the same order as the peak global transport in the northern hemisphere mid-latitudes. However, for solution  $E_{10}$ , the apparent southern boundary transport is relatively small, as the  $-2.3 \text{ Wm}^{-2}$  global bias found in this case is equivalent to about 0.6 PW in the heat transport.

#### 4.2.3 Comparison with Independent Research Buoy Measurements

In this section, we present a summary of results from a comparison of the adjusted fluxes with independent measurements from various Woods Hole Oceanographic Institute research buoys. The approach followed is the same as that described for the evaluation of the original SOC fluxes. In particular we compare the adjusted fluxes at the same location as the buoys for the period of each deployment, for further details of the buoys and the comparison method see Josey et al. (1999). One of the conclusions of the earlier evaluation was that, given the good agreement between the original SOC fluxes and the buoy measurements, adjustment of those fluxes using inverse analysis with spatially fixed changes to the free parameters would cause the revised flux estimates to diverge from the buoy values. We have investigated whether this is the case for the adjusted flux datasets obtained from the inverse analyses described earlier.

Results of the buoy comparisons are presented here for solution  $E_{10}$ , similar results are obtained when the other inverse analysis solutions are considered. Deployment mean values of the heat fluxes measured by the buoy and determined from the original and adjusted SOC datasets are listed in Table 16a-h. The amounts by which the original and adjusted fluxes differ from the research buoy values are also detailed in Table 16 and summarised graphically in Fig. 11. In the majority of cases adjustment of the SOC fluxes leads to significantly poorer agreement with the buoys. In particular, for the five Subduction buoys, the SOC - buoy net heat flux differences after adjustment lie in the range  $-30$  to  $-59 \text{ Wm}^{-2}$  compared to  $3$  to  $-19 \text{ Wm}^{-2}$  before adjustment. In contrast, at the FASINEX deployment site the adjusted latent heat flux is in better agreement with the buoy value although still underestimating the heat loss by  $21 \text{ Wm}^{-2}$  which suggests that the adjustment to this component should have been stronger in this region. For the Arabian Sea buoy

the adjustments lead to a slightly larger discrepancy than was found with the original fluxes, while at the TOGA buoy site the adjusted flux estimate is in better agreement with the buoy value. These results tend to confirm the suggestion of Josey et al. (1999) that inverse analysis with spatially fixed parameter adjustments would necessarily lead to reduced agreement between the adjusted SOC fluxes and independent buoy measurements in many of the cases considered. However, it should also be noted that the sample of buoys for which we have measurements is very small and dominated by those in the Subduction region. Despite the problems of the small sample, the results of the buoy comparisons serve as a timely warning that significant local biases exist in the adjusted fluxes, even though improved agreement has been obtained regionally with hydrography; they provide further motivation for the development of inverse analyses with spatially dependent parameter adjustments to redress this discrepancy.

## 5. SUMMARY AND DISCUSSION

The research presented in this report details initial progress towards obtaining a balanced version of the SOC climatology using inverse analysis techniques as part of a COAPEC funded project. In particular, the problem of whether it is possible to obtain a satisfactory revised set of fields with spatially fixed adjustments to the free parameters in the inverse method has been addressed. By satisfactory we mean a solution in which:

a.) the global heat budget is closed to within an amount, about  $2 \text{ Wm}^{-2}$ , which is consistent with observed decadal variations in the temperature of the near surface ocean layer (Parrilla et al., 1994).

b.) the regionally averaged net surface heat fluxes are consistent with values determined from hydrography, and

c.) the good agreement between the original SOC fluxes and independent buoy measurements is retained in the adjusted fields.

Given previous research (Josey et al., 1999) our expectation was that this goal would not be achievable but it was necessary to confirm that this was the case. At the same time the study has allowed us to become familiar with the various issues surrounding inverse analysis at an early stage of the project.

We have employed the method of linear inverse analysis with up to ten hydrographic estimates of the ocean heat transport distributed throughout the Atlantic and North Pacific oceans as constraints. Two formulations of the inverse method have been considered, the first utilises the heat transport estimates directly as constraints (Isemer et al., 1989; da Silva et al., 1994). The second is a novel application in which pairs of heat transport estimates are used to derive area averaged heat fluxes which are then employed as constraints. The solutions obtained in each case are found to be sensitive to the choice of location of the heat transport estimates when only a small number (less than 5) of constraints are applied. Consequently, we have focused on solutions obtained with the full set of ten hydrographic constraints both with and without the additional requirement that the globally averaged net flux should equal zero. We note that our desire to include as much additional information from hydrography and the various research buoys as

possible, and to include the constraint of global heat budget closure, has led us to broaden the original aim of the project from producing a balanced set of fields for the Atlantic ocean alone to a full global analysis.

The solutions obtained using all of the available heat transport constraints but not the requirement of heat budget closure have globally averaged net heat fluxes in the range  $-5$  to  $-7$   $\text{Wm}^{-2}$ . This represents a significant improvement on the strong net heat gain of  $30$   $\text{Wm}^{-2}$  that was a characteristic of the original fields but is probably still too large an imbalance given that a bias of  $1$   $\text{Wm}^{-2}$  maintained over the period of the climatology would if mixed into the upper  $1000\text{m}$  of the ocean lead to a mean temperature change of that layer by about  $0.1^\circ$  C. In order to close the global heat budget to the amount desired by a.) we have found that it is necessary to include the requirement of zero global mean net heat flux directly as an additional constraint. If it is assumed that this is an exact constraint it is possible to obtain a solution that satisfies the criterion of Isemer et al. (1989), namely that the magnitude of each of the free parameter adjustments should be less than the specified error, with the area averaged heat flux approach but not with the heat transport approach. In order to obtain a solution that satisfies this criterion with the heat transport approach it is necessary to relax the global mean constraint such that it has a non-zero error. For the case where this error is assumed to be  $2$   $\text{Wm}^{-2}$ , a solution - which we have referred to as solution  $E_{10}$  - is found with the following percentage adjustments to the different components of the heat flux : latent (19% increase), sensible (7% increase), longwave (9% increase) and shortwave (6% reduction). Given that the solutions obtained with area averaged flux constraints have to be treated with caution because of possible correlation of errors and that the heat transport solution with exact closure of the global heat budget breaks the Isemer et al. (1989) criterion, we regard solution  $E_{10}$ , which has a global mean net heat flux of  $-2.3$   $\text{Wm}^{-2}$ , as the one to be preferred from those we have obtained thus far.

For each of the solutions obtained with all ten heat transport constraints, the area averaged adjusted fluxes for each region are typically within  $\pm 20$   $\text{Wm}^{-2}$  of the hydrographic values whereas prior to the adjustment they tended to have positive biases of  $20$  -  $50$   $\text{Wm}^{-2}$ . We see this change as an improvement in that there is no longer a strong positive bias. However, it remains the case that there are regional biases of  $\pm 20$   $\text{Wm}^{-2}$  in the fluxes after the inverse calculation. In addition, comparison of the adjusted fluxes with measurements made by various WHOI research buoys reveal that the adjustments have lead to poorer agreement with the buoys in the Subduction array but better agreement with the FASINEX and TOGA buoys. This result suggests that spatially dependent parameter adjustments are required to make further progress towards obtaining a satisfactory solution.

It should be noted that in nearly all cases the differences between the regionally averaged adjusted SOC fluxes and the hydrographically implied values are within the error range determined from the uncertainties on the heat transport estimates. Thus, achieving regionally averaged fluxes which are unbiased at the  $\pm 10$   $\text{Wm}^{-2}$  level via inverse analysis is likely to require further reductions in the errors attendant on hydrographic estimates of the heat transport. New heat transport estimates are becoming available which were not employed in the present analysis e.g. Alvarez et al. (2002) now estimate the northward transport across the Fourex line from North-West Spain to the southern tip of Greenland to be  $0.65 \pm 0.1$  PW. Inclusion of this estimate in subsequent analyses will be of particular interest as it allows us to further subdivide the mid-latitude region of the North Atlantic which exhibited the strongest bias in the original SOC

climatology. In addition, the use of freshwater estimates offers us a potentially useful additional set of constraints on the analysis although the errors on such estimates remain uncomfortably large in many cases. In particular the error on the new freshwater estimate,  $-0.4 \pm 1.5$  Sv for the FOUREX line is so large as to make even the direction of the transport uncertain. Given these uncertainties, the WHOI research buoy measurements are likely to form an important additional set of constraints and we plan to employ them directly in the next step of our analysis. We note also that for the analyses reported here we have focused on the case where the adjustment parameters are simple scaling coefficients of each component of the flux. Clearly it will be important to improve the definition of the parameter error in subsequent analyses and we have already begun carrying out inverse analyses that use a spatially dependent shortwave error field which is based on the results of a separate investigation of aerosol related biases (Grist and Josey, 2002).

In conclusion, we note that our analyses with spatially dependent parameter adjustments have led to several solutions which are an improvement on the original SOC fields in that they achieve closure of the global ocean heat budget to within a few  $\text{Wm}^{-2}$  and are in better agreement with regionally averaged fluxes from hydrography. However, they have the significant problem that they are no longer in good agreement with independent measurements made by WHOI research buoys and must therefore be regarded as unsatisfactory given our long term goals for the project. We anticipate that subsequent research which incorporates spatially dependent parameter adjustments together with the buoy measurements as constraints in the analyses will allow this problem to be resolved. Despite the disagreement with the buoys we believe that the adjusted fields may prove useful as an interim globally balanced product at this stage to the COAPEC and wider research communities and will make the preferred solution noted above available to interested users.

Note: For further information on ongoing research within this project see the following website <http://www.soc.soton.ac.uk/JRD/MET/coapec.php3>

## **ACKNOWLEDGEMENTS**

The work described in this report has been funded as part of the NERC COAPEC thematic programme under the project: Balancing the Atlantic Heat and Freshwater Budgets, Ref. NER/T/S/2000/00314. We thank Peter Taylor for useful comments on this work.

## REFERENCES

- Aagaard, K. and P. Greisman, 1975: Towards new mass and heat budgets for the Arctic Ocean. *J. Geophys. Res.*, **80**, 3821 - 3827.
- Alvarez, M., Bryden, H. L., Perez, F. F., Rios, A. F., Roson, G., 2002: Physical and biogeochemical fluxes and net budgets in the Subpolar and Temperate North Atlantic. *J. Mar. Res.*, submitted.
- Bacon, S., 1997: Circulation and Fluxes in the North Atlantic between Greenland and Ireland. *J. Phys. Oceanogr.*, **27**, 1420-1435.
- Bryden, H. L., D. H. Roemmich and J. A. Church, 1991: Ocean heat transport across 24°N in the Pacific. *Deep Sea Res.* **38**, 297-324.
- da Silva, A. M., C. C. Young and S. Levitus, 1994: Atlas of Surface Marine Data Vol. 1: Algorithms and Procedures. *NOAA Atlas series*, pp.74.
- Grist, J. P. and S. A. Josey, 2002: Estimating the impact of aerosol loading on the shortwave flux fields in the SOC climatology. COAPEC Project - Balancing the Atlantic Heat and Freshwater Budgets, Report No. 2, in preparation.
- Hall, M. M. and H. L. Bryden, 1982: Direct estimates and mechanisms of ocean heat transport. *Deep - Sea Research*, **29**(3A), 339 - 359.
- Holfort, J. and G. Siedler, 2001: The meridional oceanic transports of heat and nutrients in the South Atlantic. *J. Phys. Oceanogr.*, **31**, 5-29.
- Isemer, H.-J., J. Willebrand and L. Hasse, 1989: Fine adjustment of large scale air-sea energy flux parameterizations by direct estimates of ocean heat transport. *J. Clim.*, **2**, 1173 - 1184.
- Josey, S. A., E. C. Kent and P. K. Taylor, 1998: The Southampton Oceanography Centre (SOC) Ocean - Atmosphere Heat, Momentum and Freshwater Flux Atlas. *Southampton Oceanography Centre Report No. 6, Southampton, UK*, , 30 pp. & figs.
- Josey, S. A., E. C. Kent and P. K. Taylor, 1999: New insights into the ocean heat budget closure problem from analysis of the SOC air-sea flux climatology. *J. Climate*, **12**(9), 2856 - 2880.
- Klein, B., R. L. Molinari, T. J. Mueller and G. Siedler, 1995: A transatlantic section at 14.5 N : Meridional volume and heat fluxes. *J. Mar. Res.*, **53**, 929 - 957.
- Large, W. G., G. Danabasoglu, S. C. Doney, and J. C. McWilliams, 1997: Sensitivity to surface forcing and boundary layer mixing in a global ocean model: Annual mean climatology. *J. Phys. Oceanogr.*, **27**, 2418-2447.
- Menke, W., 1984: Geophysical Data Analysis: Discrete Inverse Theory. Academic Press, 257 pp.
- Parrilla, G., A. Lavin, H. Bryden, M. Garcia, and R. Millard, 1994: Rising temperatures in the subtropical North Atlantic ocean over the past 35 years. *Nature*, **369**, 48 - 51.
- Roemmich, D. and McCallister, T, 1989: Large scale circulation of the north Pacific. *Prog. Oceanogr.*, **22**, 171-204.
- Saunders, P. M. and B. A. King, 1995: Oceanic fluxes on the WOCE A11 section. *J. Phys. Oceanogr.*, **25**, 1942-1958.

- Speer, K. G, J. Holfort, T. Reynaud, G. Siedler, 1996: South Atlantic heat Transport at 11S. *The South Atlantic: Present and Past circulation*. Springer, Berlin.
- Trenberth, K. E., J. M. Caron, and D. P. Stepaniak, 2001: The atmospheric energy budget and implications for surface fluxes and ocean heat transports. *Clim. Dyn.*, **17**, 259-276.
- Wijffels, S. E., J. M. Toole, H. L. Bryden, R. A. Fine, W. J. Jenkins, and J. L. Bullister, 1996: The water masses and circulation at 10 N in the Pacific. *Deep-Sea Research*, **1**, 501 - 544.
- WMO, 1993: International list of selected, supplementary and auxiliary ships. WMO Report, WMO, Geneva, various pagination.
- Woodruff, S. D., S. J. Lubker, K. Wolter, S. J. Worley and J. D. Elms, 1993: Comprehensive Ocean-Atmosphere Data Set (COADS) release 1a: 1980-92. *Earth System Monitor*, **4**(1), 4-8.

## APPENDIX 1. SOLUTION OF THE TWO CONSTRAINT INVERSE PROBLEM

In order to provide a check on the results of the inverse analysis obtained using the Matlab matrix inversion facility, separate results have been calculated by explicitly evaluating the solution to equation (14) for a problem with two constraints (contact Josey for full details of the calculation if required). Solutions have been obtained both for the heat transport and area averaged flux constraint approaches and this has the additional benefit of allowing us to directly compare the differences between them.

### a.) Area Averaged Flux Method

We consider the situation where we use three heat transport estimates (comprising a reference value e.g. 65° N, and two other values e.g. for the CONVEX section and 24° N in the North Atlantic) to formulate the area averaged flux constraints. The three values define two regions, which we denote by the subscripts A and B, for each of which we calculate the area averaged flux. We define region A to be the one adjacent to the reference heat transport and region B to be the more southerly of the pair (for example in the 65° N - CONVEX - 24° N case, region A would be AT08 and region B would be AT67 in Fig. 1). With the adjustable parameters for each region defined as in equation (12), the following solution vector is obtained:

$$\underline{x} = \begin{pmatrix} e_E^2 (c_A Q_{EA}^* + c_B Q_{EB}^*) \\ e_H^2 (c_A Q_{HA}^* + c_B Q_{HB}^*) \\ e_S^2 (c_A Q_{SA}^* + c_B Q_{SB}^*) \\ e_L^2 (c_A Q_{LA}^* + c_B Q_{LB}^*) \end{pmatrix} \quad (A1)$$

where,

$$c_A = b_A (\hat{Q}_{NA} - Q_{NA}^*) + b_{AB} (\hat{Q}_{NB} - Q_{NB}^*) \quad (A2)$$

$$c_B = b_{AB} (\hat{Q}_{NA} - Q_{NA}^*) + b_B (\hat{Q}_{NB} - Q_{NB}^*) \quad (A3)$$

with,

$$b_A = \left[ \sigma_A^{*2} + \hat{\sigma}_A^2 - \sigma_{AB}^{*2} / \left( \sigma_B^{*2} + \hat{\sigma}_B^2 \right) \right]^{-1} \quad (A4)$$

$$b_{AB} = \left[ \sigma_{AB}^* - \left( \sigma_A^{*2} + \hat{\sigma}_A^2 \right) \left( \sigma_B^{*2} + \hat{\sigma}_B^2 \right) / \sigma_{AB}^* \right]^{-1} \quad (A5)$$

$$b_B = \left[ \sigma_B^{*2} + \hat{\sigma}_B^2 - \sigma_{AB}^{*2} / \left( \sigma_A^{*2} + \hat{\sigma}_A^2 \right) \right]^{-1} \quad (A6)$$

and,

$$\sigma_A^{*2} = \sum_{i=1,m} e_i^2 Q_{mA}^{*2}; \quad \sigma_{AB}^* = \sum_{i=1,m} e_i^2 Q_{mA}^* Q_{mB}^*; \quad \sigma_B^{*2} = \sum_{i=1,m} e_i^2 Q_{mB}^{*2} \quad (A7)$$

b.) Heat Transport Method.

The solution obtained with the heat transport method is similar but not identical to that obtained with area averaged fluxes. The matrix  $W_E$  on the right hand side of (14) contains the same elements as in case a.) above. However, the  $W_\sigma$  matrix now contains the errors,  $\sigma_1$  and  $\sigma_2$  of the hydrographic estimates of the heat transport, and the elements of the sensitivity matrix,  $A$ , become the total heat exchange due to each flux component integrated over the area between the northern reference latitude and the relevant hydrographic section. In addition the vector,  $\mathbf{h}$ , is modified as it now contains the difference between the hydrographic and original estimates of the net heat exchange integrated over the area between the northern reference latitude and each of the hydrographic sections. Substituting for the various terms in (14) the following solution is obtained,

$$\underline{\mathbf{x}} = \begin{pmatrix} e_E^2 (d_A Q_{EA}^* + d_C Q_{EC}^*) \\ e_H^2 (d_A Q_{HA}^* + d_C Q_{HC}^*) \\ e_S^2 (d_A Q_{SA}^* + d_C Q_{SC}^*) \\ e_L^2 (d_A Q_{LA}^* + d_C Q_{LC}^*) \end{pmatrix} \quad (\text{A8})$$

where the subscript C now indicates averages over the region C formed by combining regions A and B, and

$$d_A = \beta_A S_A^2 (\hat{Q}_{NA} - Q_{NA}^*) + \beta_{AC} S_A S_C (\hat{Q}_{NC} - Q_{NC}^*) \quad (\text{A9})$$

$$d_C = \beta_C S_C^2 (\hat{Q}_{NC} - Q_{NC}^*) + \beta_{AC} S_A S_C (\hat{Q}_{NA} - Q_{NA}^*) \quad (\text{A10})$$

$S_A$  and  $S_C$  are the areas of the regions A and C respectively, and

$$\beta_A = \left[ S_A^2 \sigma_A^{*2} + \sigma_1^2 - S_A^2 \sigma_{AC}^{*2} / \left( \sigma_C^{*2} + \sigma_2^2 / S_C^2 \right) \right]^{-1} \quad (\text{A11})$$

$$\beta_{AC} = \left[ S_A S_C \sigma_{AC}^* - \left( S_A^2 \sigma_A^{*2} + \sigma_1^2 \right) \left( S_C^2 \sigma_C^{*2} + \sigma_2^2 \right) / S_A S_C \sigma_{AC}^* \right]^{-1} \quad (\text{A12})$$

$$\beta_C = \left[ S_C^2 \sigma_C^{*2} + \sigma_2^2 - S_C^2 \sigma_{AC}^{*2} / \left( \sigma_A^{*2} + \sigma_1^2 / S_A^2 \right) \right]^{-1} \quad (\text{A13})$$

with  $\sigma_A^*$  as before and,

$$\sigma_{AC}^* = \sum_{i=1,m} e_i^2 Q_{mA}^* Q_{mC}^* ; \quad \sigma_C^{*2} = \sum_{i=1,m} e_i^2 Q_{mC}^{*2} \quad (\text{A14})$$

c.) Sample Results for the 65° N - 24° N - CONVEX Case

To illustrate the differences between the solutions obtained with (A1) and (A8), we have applied them to the case where the heat transport at 65° N in the Atlantic is used as the reference value and the heat transports along the CONVEX and 24° N sections are used to form the constraints. Thus, constraints (1) and (2) from Table 1 have been used for the heat transport approach and constraints AT08 and AT67 from Table 2 for the area averaged heat flux approach. In each case the results obtained from the explicit calculation and those using Matlab are in exact agreement. However, the results obtained from the area averaged heat flux and heat

transport methods differ slightly as a result of the differences between (A1) and (A8). The numerical values of the solutions for the surface flux case are  $x_E = 0.1112$ ,  $x_H = 0.0189$ ,  $x_S = -0.1821$ ,  $x_L = 0.0696$ , whereas for the heat transport case  $x_E = 0.1141$ ,  $x_H = 0.0199$ ,  $x_S = -0.1862$ ,  $x_L = 0.0723$ . Although these differences are small they demonstrate that the two approaches to the inverse problem we have considered are not equivalent in that they give rise to slightly different adjustments.

**TABLES**

Section	Constraint no. (j)	Heat transport (PW)	Reference
CONVEX Atlantic	1	$0.28 \pm 0.06$	Bacon (1997)
24° N Atlantic	2	$1.22 \pm 0.30$	Hall and Bryden (1982)
14° N Atlantic	3	$1.22 \pm 0.42$	Klein et al (1995)
8° N Atlantic	4	$1.18 \pm 0.52$	Klein et al (1995)
11° S Atlantic	5	$0.60 \pm 0.17$	Speer et al (1996)
30° S Atlantic	6	$0.29 \pm 0.29$	Holfort and Siedler (2001)
A11 Atlantic	7	$0.46 \pm 0.16$	Saunders and King (1995)
46° N Pacific	8	$-0.09 \pm 0.30$	Roemmich and McCallister (1989)
24° N Pacific	9	$0.76 \pm 0.30$	Bryden et al (1991)
10° N Pacific	10	$0.70 \pm 0.50$	Wijffels et al.(1996)
65° N Atlantic	Northern Reference	0.1 (exact)	Aagard and Greisman (1975)
66° N Pacific	Northern Reference	0.002 (exact)	Aagard and Greisman (1975)

Table 1. Hydrographic measurements of the heat transport used for the inverse analysis. Note that the errors on the Northern Reference values are assumed to be sufficiently small that the estimates can be taken to be exact for the purpose of the analysis.

Box	Constraint No./ Label	Area (m <sup>2</sup> )	Heat flux (Wm <sup>-2</sup> ) from SOC climatology					$\hat{Q}_N$	$Q_N^* - \hat{Q}_N$
			$Q_E^*$	$Q_H^*$	$Q_S^*$	$Q_L^*$	$Q_N^*$		
CONVEX-65N	1 / AT08	2.745e+12	-59.6	-16.4	90.3	-47.8	-33.3	$-65.6 \pm 21.9$	32.3
24N-CONVEX	2 / AT67	1.833e+13	-92.8	-12.5	155.6	-52.7	-2.4	$-51.3 \pm 16.7$	48.9
14N-24N	3 / AT05	1.076e+13	-117.4	-5.8	217.6	-52.5	41.9	$0 \pm 47.9$	41.9
8N-14N	4 / AT04	3.706e+12	-117.0	-5.5	219.7	-49.5	47.8	$10.8 \pm 180.4$	37.0
11S -8N	5 / AT03	1.225e+13	-99.0	-4.2	221.3	-48.6	69.5	$47.5 \pm 44.8$	22.0
30S-11S	6 / AT02	1.221e+13	-100.7	-4.8	202.6	-53.6	43.5	$25.4 \pm 27.5$	18.1
A11-30S	7 / AT01	8.416e+12	-77.2	-6.5	157.1	-53.4	20.0	$-25.0 \pm 36.5$	45.0
46N-66N	8 / PA01	6.747e+12	-36.2	-9.3	98.0	-40.0	12.6	$13.6 \pm 44.5$	-1.0
24N-46N	9 / PA02	2.607e+13	-89.9	-11.6	159.8	-50.4	7.9	$-32.6 \pm 16.3$	40.5
10N -24N	10 / PA03	2.491e+13	-115.5	-6.8	214.2	-48.4	43.5	$2.4 \pm 23.4$	41.1
Global Ocean	-	3.224e+14	-92.2	-7.2	179.5	-49.7	30.4	$0 \pm 0$	30.4

Table 2. Details of the regions used for the area averaged flux approach. The area averaged values of the original SOC fluxes are listed for each region together with the net heat flux implied by hydrography,  $\hat{Q}_N$ , and the difference  $Q_N^* - \hat{Q}_N$ , flux units are Wm<sup>-2</sup>.

	Latent	Sensible	Shortwave	Longwave	Net
$Q_i^*$	-92.2	-7.2	179.5	-49.7	30.4
$e_i$	0.2	0.2	0.2	0.2	-
$x_i$	0.065	0.005	-0.126	0.035	-
$dQ_i^*$	-6.0	0.0	-22.6	-1.8	-30.4
Adjusted flux	-98.2	-7.2	156.9	-51.5	0.0

Table 3. Results of inverse analysis with the single constraint of global closure of the SOC flux climatology, according to scenario 1 for the parameter errors ( $e_i$ ), note  $dQ_i^*$  is the amount by which each component of the heat flux is adjusted.

	Latent	Sensible	Shortwave	Longwave	Net
$Q_i^*$	-92.2	-7.2	179.5	-49.7	30.4
$e_i$	0.2	0.2	0.1	0.1	-
$x_i$	0.163	0.0127	-0.0792	0.0219	-
$dQ_i^*$	-15.0	0.1	-14.2	-1.1	-30.4
Adjusted flux	-107.2	-7.3	165.3	-50.8	0.0

Table 4. Results of inverse analysis with the single constraint of global closure of the SOC flux climatology, according to scenario 2 for the parameter errors ( $e_i$ ).

	Latent	Sensible	Shortwave	Longwave	Net
$Q_i^*$	-92.2	-7.2	179.5	-49.7	30.4
$e_i$	0.1	0.1	0.2	0.2	-
$x_i$	0.019	0.002	-0.148	0.041	-
$dQ_i^*$	-1.8	0.0	-26.6	-2.0	-30.4
Adjusted flux	-94.0	-7.2	152.9	-51.7	0.0

Table 5. Results of inverse analysis with the single constraint of global closure of the SOC flux climatology, according to scenario 3 for the parameter errors ( $e_i$ ).

No. of Constraints	$dp_E$	$dp_H$	$dp_S$	$dp_L$
1	0.07	0.02	-0.11	0.06
2	0.11	0.02	-0.19	0.07
3	0.11	0.02	-0.18	0.07
4	0.11	0.02	-0.18	0.07
5	0.12	0.04	-0.12	0.10
6	0.13	0.05	-0.11	0.10
7	0.14	0.05	-0.09	0.09
8	0.14	0.05	-0.09	0.09
9	0.14	0.05	-0.09	0.10
10 (Solution $A_{10}$ )	0.15	0.06	-0.09	0.09

Table 6. Solutions for case A heat transport approach without the requirement of global closure.

No. of Constraints	$dp_E$	$dp_H$	$dp_S$	$dp_L$
1	0.07	0.02	-0.11	0.06
2	0.11	0.02	-0.18	0.07
3	0.11	0.02	-0.17	0.07
4	0.11	0.02	-0.17	0.07
5	0.11	0.03	-0.15	0.08
6	0.11	0.04	-0.12	0.08
7	0.11	0.04	-0.12	0.08
8	0.11	0.03	-0.12	0.08
9	0.12	0.04	-0.12	0.08
10 (Solution $B_{10}$ )	0.12	0.04	-0.12	0.08

Table 7. Solutions for case B area averaged flux approach without the requirement of global closure.

No. of Constraints	$dp_E$	$dp_H$	$dp_S$	$dp_L$
1	0.08	0.02	-0.11	0.06
2	0.11	0.04	-0.09	0.09
3	0.13	0.05	-0.07	0.10
4	0.15	0.06	-0.06	0.10
5	0.20	0.08	-0.04	0.08
6	0.21	0.08	-0.04	0.07
7	0.23	0.08	-0.03	0.07
8	0.23	0.08	-0.03	0.07
9	0.24	0.09	-0.02	0.08
10 (Solution C <sub>10</sub> )	0.25	0.09	-0.02	0.08

Table 8. Solutions for case C heat transport approach with the requirement of global closure.

No. of Constraints	$dp_E$	$dp_H$	$dp_S$	$dp_L$
1	0.07	0.02	-0.11	0.06
2	0.10	0.04	-0.09	0.08
3	0.10	0.04	-0.09	0.08
4	0.10	0.04	-0.09	0.08
5	0.10	0.04	-0.09	0.08
6	0.11	0.04	-0.09	0.08
7	0.10	0.04	-0.09	0.09
8	0.11	0.04	-0.09	0.08
9	0.12	0.05	-0.08	0.09
10 (Solution D <sub>10</sub> )	0.12	0.05	-0.08	0.09

Table 9. Solutions for case D area averaged flux approach with the requirement of global closure.

Box	Hydrographic estimate	Difference of area averaged fluxes (SOC-Hydrographic)									
		Number of constraints used									
		1	2	3	4	5	6	7	8	9	10
AT08 (CONVEX-65N)	$-65.6 \pm 21.9$	14.7	4.9	5.4	5.9	9.0	9.6	10.2	10.3	10.1	9.3
AT67 (24N-CONVEX)	$-51.3 \pm 16.7$	21.4	5.2	6.2	7.0	13.4	14.8	15.9	15.9	15.7	14.9
AT05 (14N-24N)	$0 \pm 47.9$	4.0	-15.9	-14.6	-13.4	-3.7	-1.5	0.1	0.1	0.1	-0.8
AT04 (8N-14N)	$10.8 \pm 180.4$	1.0	-21.0	-9.6	-18.5	-8.6	-6.3	-4.7	-4.7	-4.7	-5.5
AT03 (11S -8N)	$47.5 \pm 44.8$	-12.8	-34.1	-32.8	-31.7	-21.5	-19.0	-17.2	-17.2	-17.1	-17.9
AT02 (30S-11S)	$25.4 \pm 27.5$	-15.0	-35.1	-33.8	-32.8	-23.8	-21.6	-20.0	-20.0	-20.0	-20.9
AT01 (A11-30S)	$-20.3 \pm 39.2$	13.9	-1.8	-0.8	0.0	6.7	8.3	9.4	9.7	9.6	8.8
PA01 (46N-66N)	$13.6 \pm 44.5$	-17.1	-26.5	-25.9	-25.5	-21.4	-20.4	-19.4	-19.3	-19.4	-20.0
PA02 (24N-46N)	$-32.6 \pm 16.3$	13.0	-3.4	-2.4	-1.6	5.1	6.6	7.8	7.8	7.7	6.9
PA03 (10N -24N)	$2.4 \pm 23.4$	5.9	-15.6	-14.3	-13.2	-3.4	-1.4	0.2	0.1	0.1	-0.6
Global Ocean	$0 \pm 2$	0.6	-17.3	-16.2	-15.3	-7.4	-5.6	-4.2	-4.2	-4.2	-5.0

Table 10. Case A differences between the adjusted SOC estimate and the hydrographic estimate of the area averaged heat flux for the various regions considered, flux units are  $\text{Wm}^{-2}$ .

Box	Hydrographic estimate	Difference of area averaged fluxes (SOC - Hydrographic)									
		Number of constraints used									
		1	2	3	4	5	6	7	8	9	10
AT08 (CONVEX-65N)	$-65.6 \pm 21.9$	14.7	5.6	6.3	6.4	7.9	10.7	10.3	10.7	9.4	9.6
AT67 (24N-CONVEX)	$-51.3 \pm 16.7$	21.4	6.3	7.7	7.9	10.7	15.7	15.2	15.8	13.6	14.1
AT05 (14N-24N)	$0 \pm 47.9$	4.0	-14.5	-12.4	-12.2	-8.0	-0.9	-1.6	-0.9	-3.7	-3.0
AT04 (8N-14N)	$10.8 \pm 180.4$	1.0	-19.6	-17.5	-17.3	-13.0	-5.8	-6.5	-5.8	-8.6	-7.8
AT03 (11S-8N)	$47.5 \pm 44.8$	-12.8	-32.8	-30.7	-30.5	-26.1	-18.9	-19.7	-18.8	-21.5	-20.8
AT02 (30S-11S)	$25.4 \pm 27.5$	-15.0	-33.8	-31.9	-31.7	-27.8	-21.2	-21.9	-21.1	-23.7	-23.0
AT01 (A11-30S)	$-20.3 \pm 39.2$	13.9	-0.7	0.7	0.8	3.8	8.9	8.3	8.9	6.9	7.4
PA01 (46N-66N)	$13.6 \pm 44.5$	-17.1	-25.9	-25.0	-25.0	-23.1	-20.1	-20.4	-19.9	-21.1	-20.9
PA02 (24N-46N)	$-32.6 \pm 16.3$	13.0	-2.3	-0.8	-0.7	2.3	7.4	6.8	7.5	5.3	5.8
PA03 (10N-24N)	$2.4 \pm 23.4$	5.9	-14.23	-12.2	-12.0	-7.8	-0.8	-1.6	-0.8	-3.6	-2.9
Global Ocean	$0 \pm 2$	0.6	-16.1	-14.5	-14.3	-10.9	-5.0	-5.7	-5.0	-7.3	-6.7

Table 11. Case B differences between the adjusted SOC estimate and the hydrographic estimate of the area averaged heat flux for the various regions considered, flux units are  $\text{Wm}^{-2}$

Box	Hydrographic estimate	Difference of area averaged fluxes (SOC- Hydrographic)									
		Number of constraints used									
		1	2	3	4	5	6	7	8	9	10
AT08 (CONVEX-65N)	$-65.6 \pm 21.9$	14.4	12.9	12.3	11.9	11.6	11.6	11.3	11.3	10.8	10.7
AT67 (24N-CONVEX)	$-51.3 \pm 16.7$	20.9	20.0	19.5	19.2	18.7	18.7	18.3	18.3	18.1	18.0
AT05 (14N-24N)	$0 \pm 47.9$	5.2	5.3	5.3	5.2	4.8	4.7	4.6	4.6	4.7	4.7
AT04 (8N-14N)	$10.8 \pm 180.4$	0.2	0.5	0.4	0.6	0.1	0.1	-0.1	-0.1	0.1	0.1
AT03 (11S -8N)	$47.5 \pm 44.8$	-13.6	-12.5	-12.1	-11.8	-11.2	-11.2	-10.8	-10.8	-10.5	-10.4
AT02 (30S-11S)	$25.4 \pm 27.5$	-15.7	-15.4	-15.3	-15.2	-15.1	-15.0	-15.0	-15.0	-14.4	-14.8
AT01 (A11-30S)	$-20.3 \pm 39.2$	13.4	13.2	13.1	13.2	13.6	13.7	13.8	13.8	13.7	-13.8
PA01 (46N-66N)	$13.6 \pm 44.5$	-17.4	-17.5	-17.4	-17.2	-16.2	-16.1	-15.7	-15.6	-15.8	-15.7
PA02 (24N-46N)	$-32.6 \pm 16.3$	12.9	11.8	11.5	11.3	11.0	11.0	10.8	10.8	10.6	10.6
PA03 (10N -24N)	$2.4 \pm 23.4$	5.1	5.3	5.3	5.2	4.7	4.7	4.5	4.4	4.6	4.6
Global Ocean	$0 \pm 0$	0	0	0	0	0	0	0	0	0	0

Table 12. Case C differences between the adjusted SOC estimate and the hydrographic estimate of the area averaged heat flux for the various regions considered, flux units are  $\text{Wm}^{-2}$

Box	Hydrographic estimate	Difference of area averaged fluxes (SOC- Hydrographic)									
		Number of constraints used									
		1	2	3	4	5	6	7	8	9	10
AT08 (CONVEX-65N)	$-65.6 \pm 21.9$	14.4	13.4	13.4	13.4	13.3	13.2	13.1	13.2	12.8	12.9
AT67 (24N-CONVEX)	$-51.3 \pm 16.7$	20.9	20.2	20.2	20.2	20.2	20.1	20.1	20.1	19.9	19.9
AT05 (14N-24N)	$0 \pm 47.9$	5.2	5.3	5.3	5.3	5.3	5.2	5.2	5.2	5.1	5.1
AT04 (8N-14N)	$10.8 \pm 180.4$	0.2	0.4	0.4	0.4	0.40	0.4	0.5	0.4	0.5	0.4
AT03 (11S -8N)	$47.5 \pm 44.8$	-13.6	-12.8	-12.9	-12.9	-12.8	-12.7	-12.7	-12.7	-12.4	-12.4
AT02 (30S-11S)	$25.4 \pm 27.5$	-15.7	-15.5	-15.5	-15.5	-15.5	-15.5	-15.5	-15.4	-15.4	-15.4
AT01 (A11-30S)	$-20.3 \pm 39.2$	13.4	13.2	13.2	13.2	13.2	13.2	13.2	13.2	13.2	13.3
PA01 (46N-66N)	$13.6 \pm 44.5$	-17.4	-17.4	-17.4	-17.4	-17.4	-17.4	-17.5	-17.3	-17.4	-17.3
PA02 (24N-46N)	$-32.6 \pm 16.3$	12.4	12.0	12.0	12.0	11.9	11.9	11.9	11.9	11.7	11.8
PA03 (10N -24N)	$2.4 \pm 23.4$	5.1	5.2	5.2	5.2	5.2	5.2	5.3	5.2	5.2	5.2
Global Ocean	$0 \pm 0$	0	0	0	0	0	0	0	0	0	0

Table 13. Case D differences between the adjusted SOC estimate and the hydrographic estimate of the area averaged heat flux for the various regions considered, flux units are  $\text{Wm}^{-2}$

No. of Constraints	$dp_E$	$dp_H$	$dp_S$	$dp_L$
1	0.08	0.02	-0.11	0.06
2	0.11	0.04	-0.09	0.09
3	0.13	0.05	-0.08	0.10
4	0.15	0.06	-0.07	0.10
5	0.18	0.07	-0.06	0.08
6	0.18	0.07	-0.06	0.08
7	0.18	0.07	-0.06	0.08
8	0.19	0.06	-0.06	0.08
9	0.19	0.07	-0.06	0.09
10 (Solution $E_{10}$ )	0.19	0.07	-0.06	0.09

Table 14. Solutions for case E heat transport approach with the requirement that the global net heat flux equal  $0 \pm 2 \text{ Wm}^{-2}$ .

Box	Hydrographic estimate	Difference of area averaged fluxes (SOC- Hydrographic)									
		Number of Constraints used									
		1	2	3	4	5	6	7	8	9	10
AT08 (CONVEX-65N)	-65.6 ± 21.9	14.4	12.7	12.0	11.6	10.9	11.0	10.7	10.7	10.4	10.3
AT67 (24N-CONVEX)	-51.3 ± 16.7	20.8	19.6	19.1	18.6	17.3	17.4	17.0	16.9	16.8	16.7
AT05 (14N-24N)	0 ± 47.9	5.1	4.9	4.7	4.3	2.6	2.8	2.2	2.1	2.2	2.1
AT04 (8N-14N)	10.8 ± 180.4	0.2	0.1	0.0	-0.4	-2.1	-1.9	-2.5	-2.7	-2.5	-2.6
AT03 (11S -8N)	47.5 ± 44.8	-13.6	-13.0	-12.7	-12.7	-13.8	-13.7	-14.2	-14.3	-14.0	-14.1
AT02 (30S-11S)	25.4 ± 27.5	-15.8	-15.9	-15.9	-16.1	-17.3	-17.1	-17.7	-17.8	-17.6	-17.7
AT01 (A11-30S)	-20.3 ± 39.2	13.4	12.9	12.8	12.6	11.9	12.0	11.6	11.5	11.5	11.5
PA01 (46N-66N)	13.6 ± 44.5	-17.5	-17.7	-17.6	-17.6	-17.5	-17.5	-17.7	-17.6	-17.8	-17.7
PA02 (24N-46N)	-32.6 ± 16.3	12.3	11.5	11.1	10.7	9.5	9.6	9.2	9.1	9.1	9.0
PA03 (10N -24N)	2.4 ± 23.4	5.0	4.9	4.7	4.3	2.6	2.8	2.2	2.0	2.2	2.1
Global Ocean	0 ± 2	-0.1	-0.4	-0.5	-0.8	-1.9	-1.8	-2.2	-2.3	-2.2	-2.3

Table 15. Case E differences between the adjusted SOC estimate and the hydrographic estimate of the area averaged heat flux for the various regions considered, flux units are  $Wm^{-2}$

NE Buoy (33°N, 22°W)

	Latent	Sensible	Shortwave	Longwave	Net
Buoy	-95	-9	195	-66	25
SOC (SOC -buoy )	-91 (4)	-6 (3)	182 (-13)	-57 (-9)	28 (3)
Solution E <sub>10</sub> (Sln. E <sub>10</sub> -buoy)	-109 (-14)	-6 (3)	172 (-23)	-62 (4)	-5 (-30)

Table 16a. Comparison of the various flux components obtained from the NE subduction array buoy (Buoy), the original SOC climatology (SOC) and the climatology adjusted according to Solution E<sub>10</sub> (Sln. E<sub>10</sub>).

SE Buoy (18°N, 22°W)

	Latent	Sensible	Shortwave	Longwave	Net
Buoy	-101	-7	209	-47	54
SOC (SOC -buoy )	-106 (-5)	-6 (1)	222 (13)	-56 (-9)	54 (0)
Solution E <sub>10</sub> (Sln. E <sub>10</sub> -buoy)	-127 (-26)	-6 (1)	210 (-1)	-61 (-14)	16 (-38)

Table 16b. Comparison of the various flux components obtained from the SE subduction array buoy (Buoy), the original SOC climatology (SOC) and the climatology adjusted according to Solution E<sub>10</sub> (Sln. E<sub>10</sub>).

SW Buoy (18°N, 34°W)

	Latent	Sensible	Shortwave	Longwave	Net
Buoy	-128	-5	233	-58	42
SOC (SOC -buoy )	-128 (0)	-9 (-4)	217 (-16)	-54 (4)	26 (-16)
Solution E <sub>10</sub> (Sln. E <sub>10</sub> -buoy)	-153 (-25)	-9 (-4)	204 (-29)	-59 (-1)	-17 (-59)

Table 16c. Comparison of the various flux components obtained from the SW subduction array buoy (Buoy), the original SOC climatology (SOC) and the climatology adjusted according to Solution E<sub>10</sub> (Sln. E<sub>10</sub>).

NW Buoy (33°N, 34°W)

	Latent	Sensible	Shortwave	Longwave	Net
Buoy	-85	-7	196	-76	28
SOC (SOC -buoy )	-99 (-14)	-7 (0)	182 (-14)	-56 (20)	20 (-8)
Solution E <sub>10</sub> (Sln. E <sub>10</sub> -buoy)	-118 (-33)	-7 (0)	171 (-25)	-61 (15)	-15 (-43)

Table 16d. Comparison of the various flux components obtained from the NW subduction array buoy (Buoy), the original SOC climatology (SOC) and the climatology adjusted according to Solution E<sub>10</sub> (Sln. E<sub>10</sub>).

C Buoy (33°N, 34°W)

	Latent	Sensible	Shortwave	Longwave	Net
Buoy	-106	-7	214	-65	36
SOC (SOC -buoy )	-115 (-9)	-8 (-1)	199 (-15)	-59 (6)	17 (-19)
Solution E <sub>10</sub> (Sln. E <sub>10</sub> -buoy)	-137 (-31)	-8 (-1)	187 (-27)	-64 (1)	-22 (-58)

Table 16e. Comparison of the various flux components obtained from the Central subduction array buoy (Buoy), the original SOC climatology (SOC) and the climatology adjusted according to Solution E<sub>10</sub> (Sln. E<sub>10</sub>).

FASINEX buoy (27°N, 70°W)

	Latent	Sensible	Shortwave	Longwave	Net
Buoy	-170	-17	222	---	---
SOC (SOC -buoy )	-125 (45)	-10 (7)	220 (-2)	-63 (---)	22 (--)
Solution E <sub>10</sub> (Sln. E <sub>10</sub> -buoy)	-149 (21)	-11 (6)	208 (-14)	-69	-21

Table 16f. Comparison of the various flux components obtained from the FASINEX buoy (Buoy), the original SOC climatology (SOC) and the climatology adjusted according to Solution E<sub>10</sub> (Sln. E<sub>10</sub>). Note that longwave measurements were not made on this deployment.

TOGA buoy (1.75°S, 156°E)

	Latent	Sensible	Shortwave	Longwave	Net
Buoy	-108	-9	196	-58	21
SOC (SOC -buoy )	-115 (-7)	-10 (-1)	219 (23)	-50 (8)	44 (23)
Solution E <sub>10</sub> (Sln. E <sub>10</sub> -buoy)	-136 (-28)	-10 (-1)	208 (12)	-54 (4)	8 (-13)

Table 16g. Comparison of the various flux components obtained from the TOGA buoy (Buoy), the original SOC climatology (SOC) and the climatology adjusted according to Solution E<sub>10</sub> (Sln. E<sub>10</sub>).

Arabian Sea Buoy (15.5°N, 61.5°E)

	Latent	Sensible	Shortwave	Longwave	Net
Buoy	-121	-2	243	-59	61
SOC (SOC -buoy )	-110 (11)	-1 (1)	240 (-3)	-51 (8)	78 (17)
Solution E <sub>10</sub> (Sln. E <sub>10</sub> -buoy)	-131 (-20)	-1 (1)	226 (-17)	-56 (3)	38 (-23)

Table 16h. Comparison of the various flux components obtained from the Arabian Sea buoy (Buoy), the original SOC climatology (SOC) and the climatology adjusted according to Solution E<sub>10</sub> (Sln. E<sub>10</sub>).

## FIGURE CAPTIONS

Figure 1. Map showing the location of the constraints used in the study. Sections for which hydrographic heat transport estimates have been employed as constraints are numbered 1-10. Regions for which the area averaged net heat flux derived from hydrography is used as a constraint are labelled e.g. AT01, AT02.

Figure 2. Dependence of the parameter adjustments, on the sequence of constraints used for the inverse analysis. The constraint number variable on the x-axis indicates the number of constraints in the sequence presented in Tables 1 and 2 that have been used for the analysis. The separate panels summarise the various solutions obtained for  $\mathbf{x}_i$  for analyses in which a) the global net heat flux has not been constrained to equal zero; b) the global net heat flux has been constrained to equal zero, and c) the global net heat flux has been constrained to be  $0 \pm 2 \text{ Wm}^{-2}$ . The adjustments for the different parameters are indicated by colour as follows: latent heat (green), longwave (black), sensible heat (red) and shortwave (blue), while crosses indicate results obtained with the heat transport approach and circles indicate the area averaged flux approach.

Figure 3. Maps showing the difference (adjusted -original) between the adjusted and original SOC heat flux components for Solution  $A_{10}$  (units  $\text{Wm}^{-2}$ ). Note that panels a) and c) have a different scale to b) and d).

Figure 4. Maps showing the difference (adjusted -original) between the adjusted and original SOC heat flux components for Solution  $B_{10}$  (units  $\text{Wm}^{-2}$ ). Note that panels a) and c) have a different scale to b) and d).

Figure 5. Maps showing the difference (adjusted -original) between the adjusted and original SOC net heat flux components for Solutions  $A_{10}$  to  $E_{10}$  (units  $\text{Wm}^{-2}$ ).

Figure 6. Maps showing the difference (adjusted -original) between the adjusted and original SOC heat flux components for Solution  $C_{10}$  (units  $\text{Wm}^{-2}$ ). Note that panels a) and c) have a different scale to b) and d).

Figure 7. Maps showing the difference (adjusted -original) between the adjusted and original SOC heat flux components for Solution  $D_{10}$  (units  $\text{Wm}^{-2}$ ). Note that panels a) and c) have a different scale to b) and d).

Figure 8. Maps showing the difference (adjusted -original) between the adjusted and original SOC heat flux components for Solution  $E_{10}$  (units  $\text{Wm}^{-2}$ ). Note that panels a) and c) have a different scale to b) and d).

Figure 9. Schematic representation of the difference (SOC-hydrography) between the area averaged heat flux from the SOC climatology and that implied by hydrography for a) the original SOC climatology and b) the SOC climatology adjusted according to solution  $E_{10}$  (units  $\text{Wm}^{-2}$ ).

Figure 10. Climatologically implied ocean heat transport for a) the Atlantic Ocean, b) the Pacific Ocean and c) the Global Ocean for the original SOC climatology (red line), solution  $A_{10}$  (green), solution  $B_{10}$  (blue), solution  $C_{10}$  (black), solution  $D_{10}$  (magenta) and solution  $E_{10}$  (cyan). Blue crosses indicate hydrographic estimates of the heat transport.

Figure 11. Summary plot showing the difference between the SOC estimates and WHOI research buoy measurements of the various heat flux components and the net heat flux. Left hand column : differences between the original SOC climatology and the buoys. Right hand column : differences between adjusted SOC Solution  $E_{10}$  and the buoys. The numbers refer to the different buoys considered as follows: 1 - NE buoy (subduction array); 2 - SE buoy (subduction array); 3 - SW buoy (subduction array); 4 - NW buoy (subduction array); 5 - Central buoy (subduction array); 6 - FASINEX buoy; 7 - TOGA buoy; 8 - Arabian Sea Buoy. Note that buoy measurements of the longwave and net heat flux were not available for FASINEX.

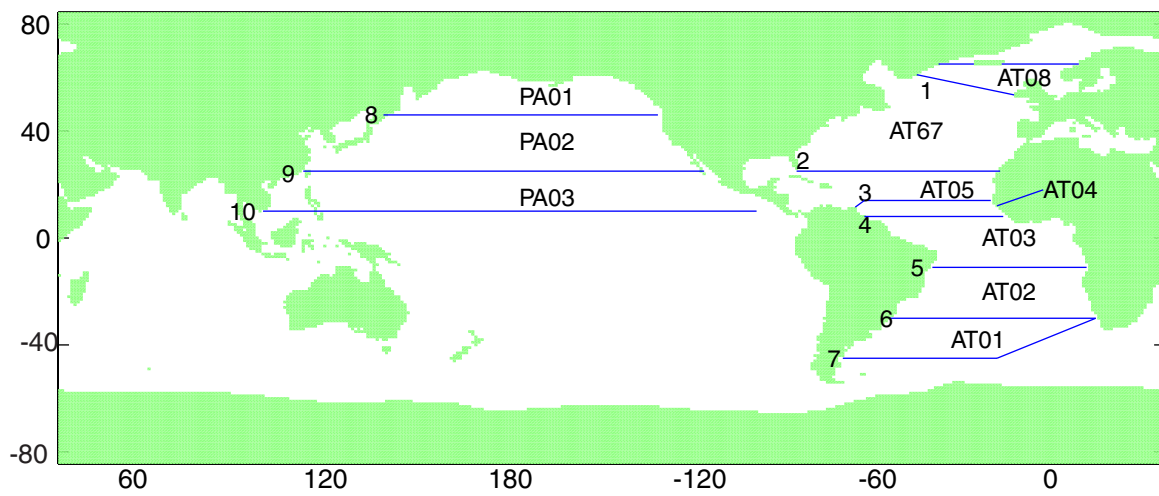


Figure 1. Map showing the locations of constraints used in the study. Sections for which hydrographic heat transport estimates have been employed as constraints are numbered 1-10. Regions for which the area averaged net heat flux derived from hydrography is used as a constraint are labelled AT01, AT02 etc.

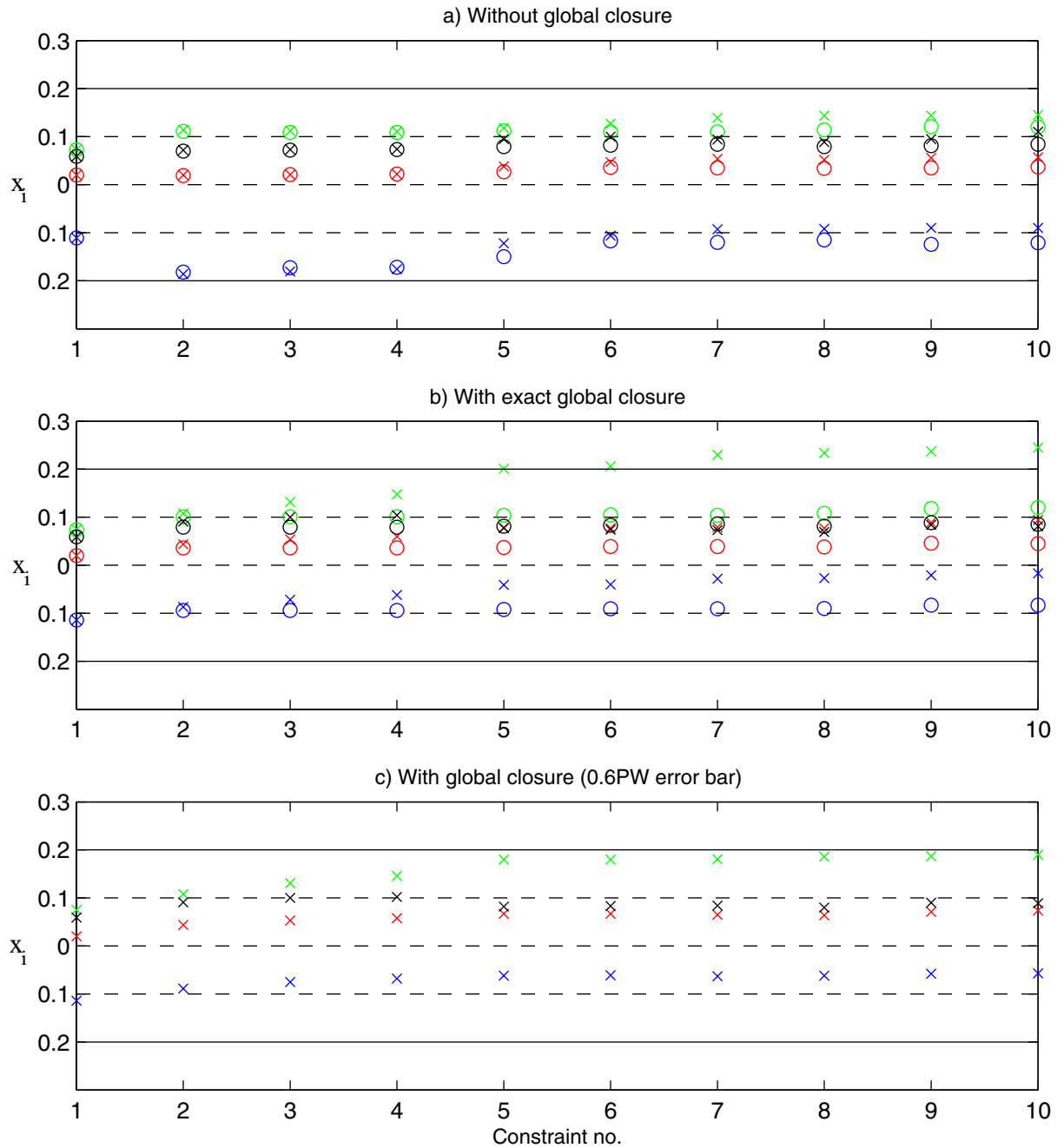


Figure 2. Dependence of the parameter adjustments, on the sequence of constraints used for the inverse analysis. The constraint number variable on the x-axis indicates the number of constraints in the sequence presented in Tables 1 and 2 that have been used for the analysis. The separate panels summarise the various solutions obtained for  $x_1$  for analyses in which a) the global net heat flux has not been constrained to equal zero; b) the global net heat flux has been constrained to equal zero, and c) the global net heat flux has been constrained to be  $0 \pm 2 \text{ Wm}^{-2}$ . The adjustments for the different parameters are indicated by colour as follows: latent heat (green), longwave (black), sensible heat (red) and shortwave (blue), while crosses indicate results obtained with the heat transport approach and circles indicate the area averaged flux approach.

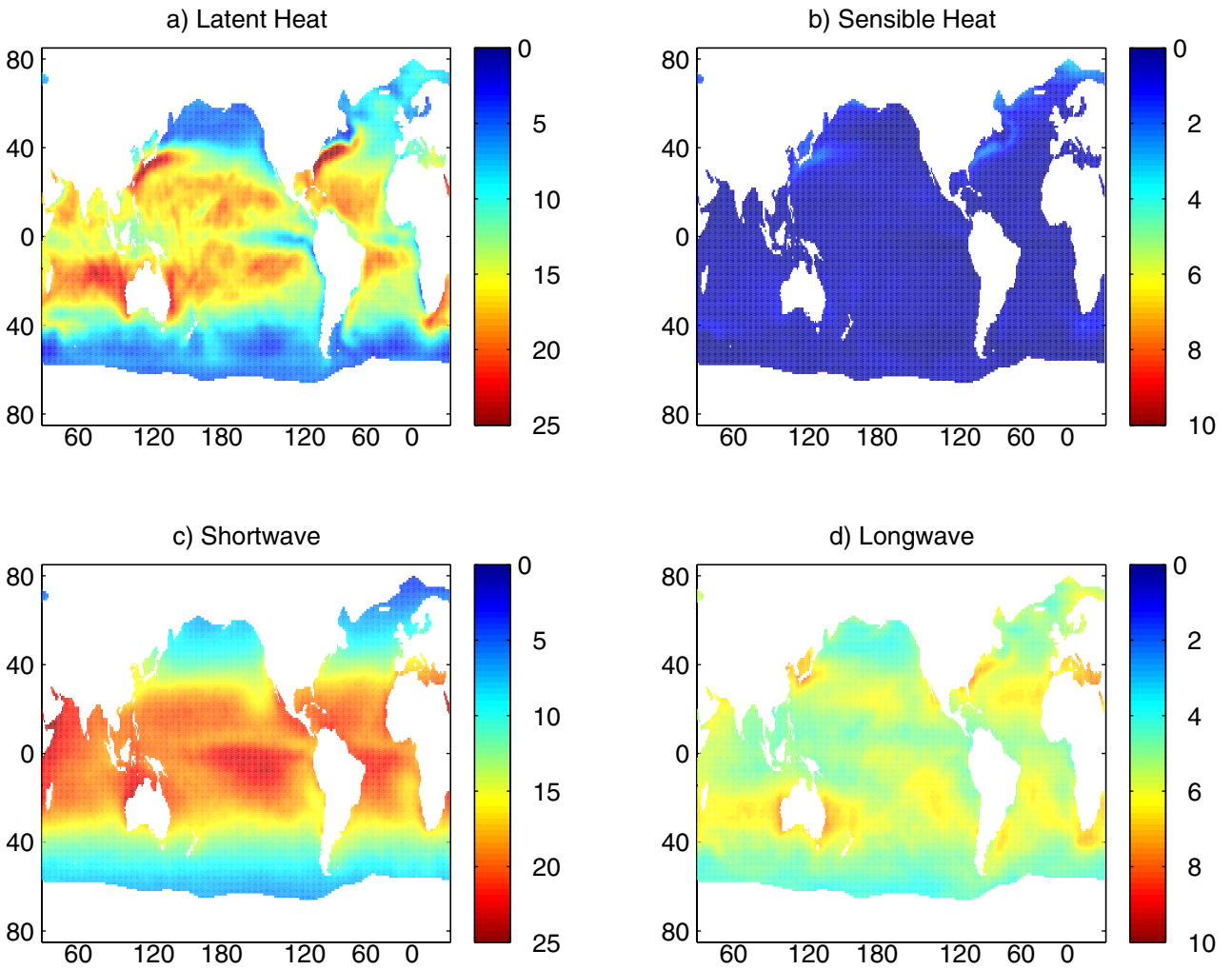


Figure 3. Maps showing the difference (adjusted -original) between the adjusted and original SOC heat flux components for Solution A<sub>10</sub> (units W/m<sup>2</sup>). Note that panels a) and c) have a different scale to b) and d)

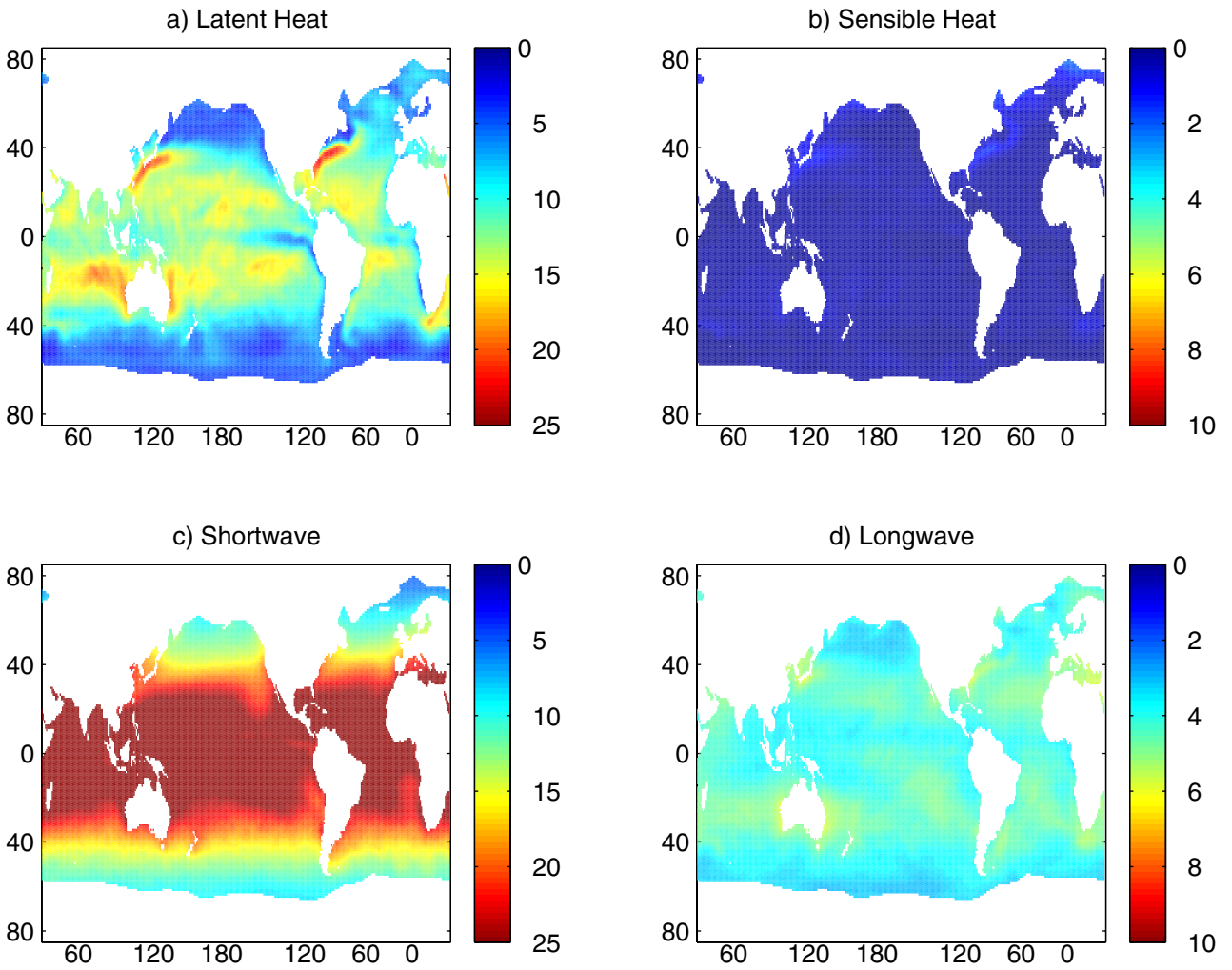
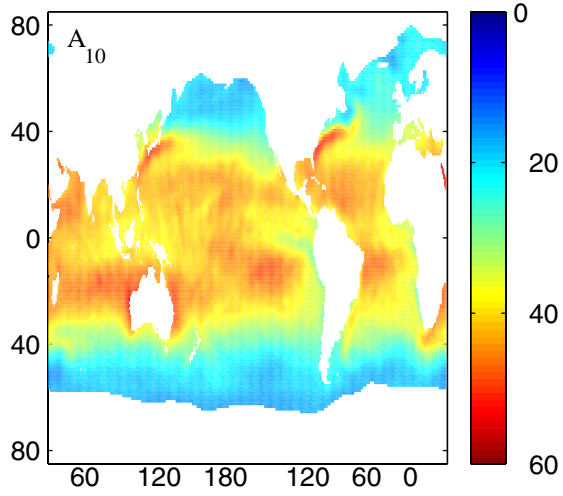
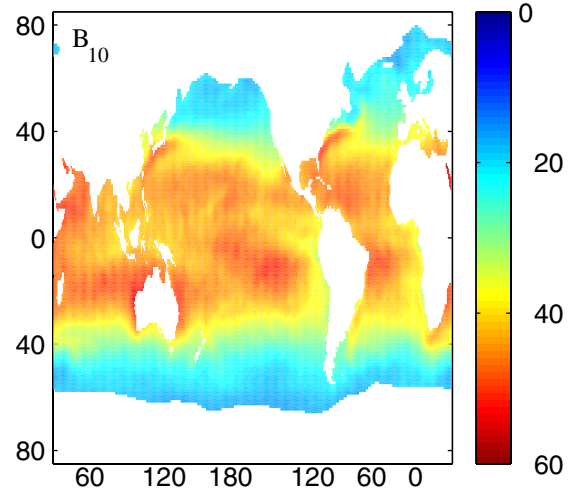


Figure 4. Maps showing the difference (adjusted -original) between the adjusted and original SOC heat flux components for Solution B<sub>10</sub> (units W/m<sup>2</sup>). Note that panels a) and c) have a different scale to b) and d).

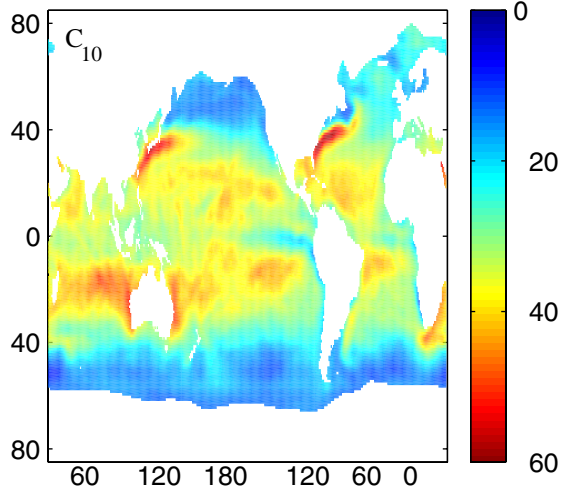
a) Heat transport method no global closure



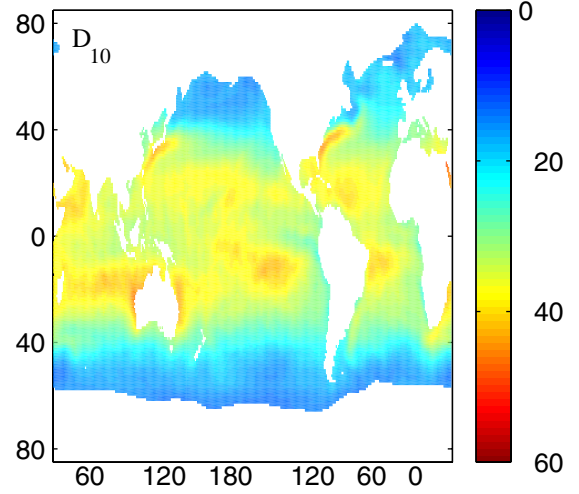
b) Flux method no global closure



c) Heat transport method global closure



d) Flux method global closure



e) Heat Transport method global closure with  $2\text{Wm}^{-2}$  error

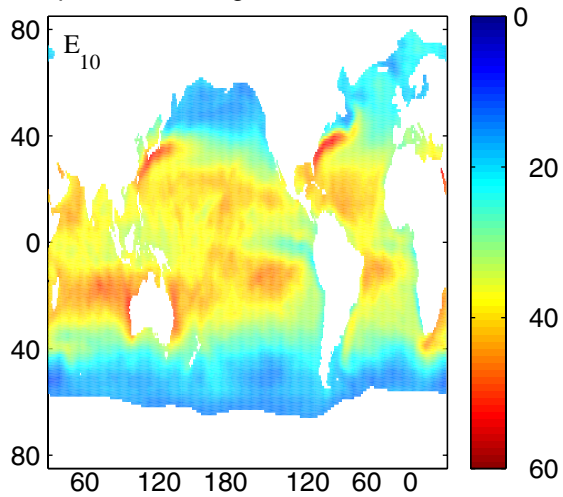


Figure 5. Maps showing the difference (adjusted - original) between the adjusted and original SOC net heat flux components for solutions  $A_{10}$  to  $E_{10}$  (units  $\text{W}/\text{m}^2$ ).

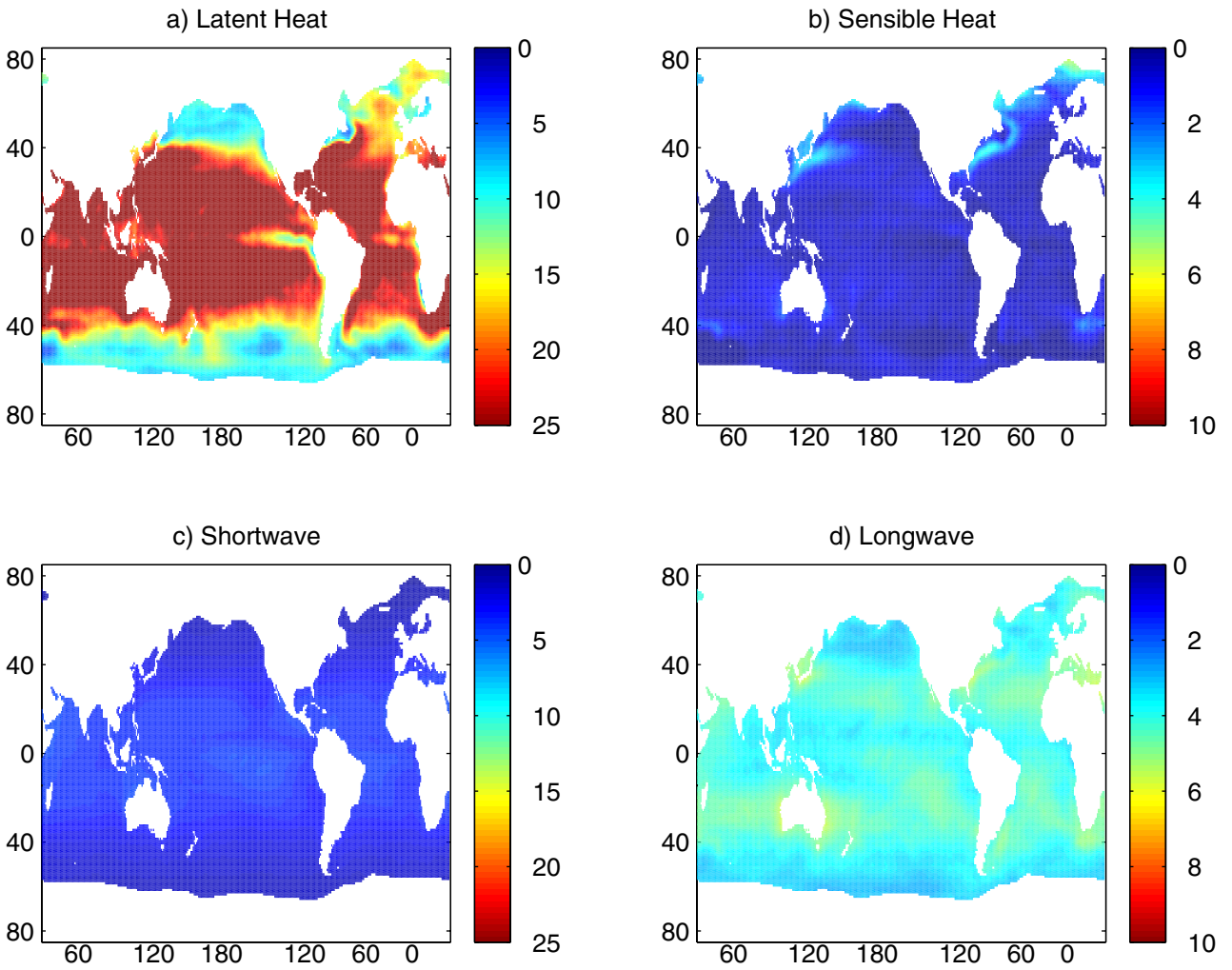


Figure 6. Maps showing the difference (adjusted -original) between the adjusted and original SOC heat flux components for Solution C (units W/m<sup>2</sup>). Note that panels a) and c) have a different scale to b) and d)

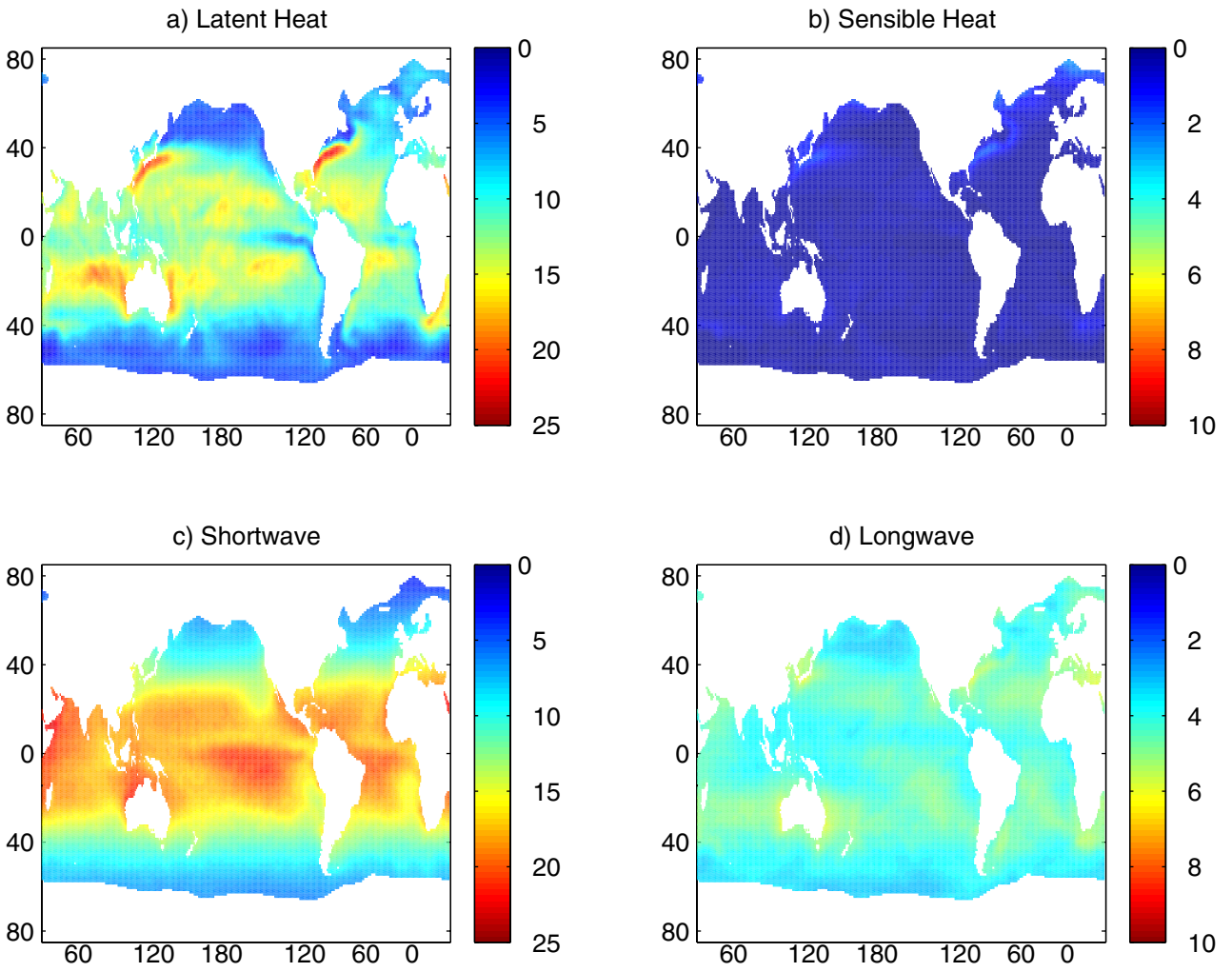


Figure 7. Maps showing the difference (adjusted -original) between the adjusted and original SOC heat flux components for Solution D (units W/m<sup>2</sup>). Note that panels a) and c) have a different scale to b) and d)

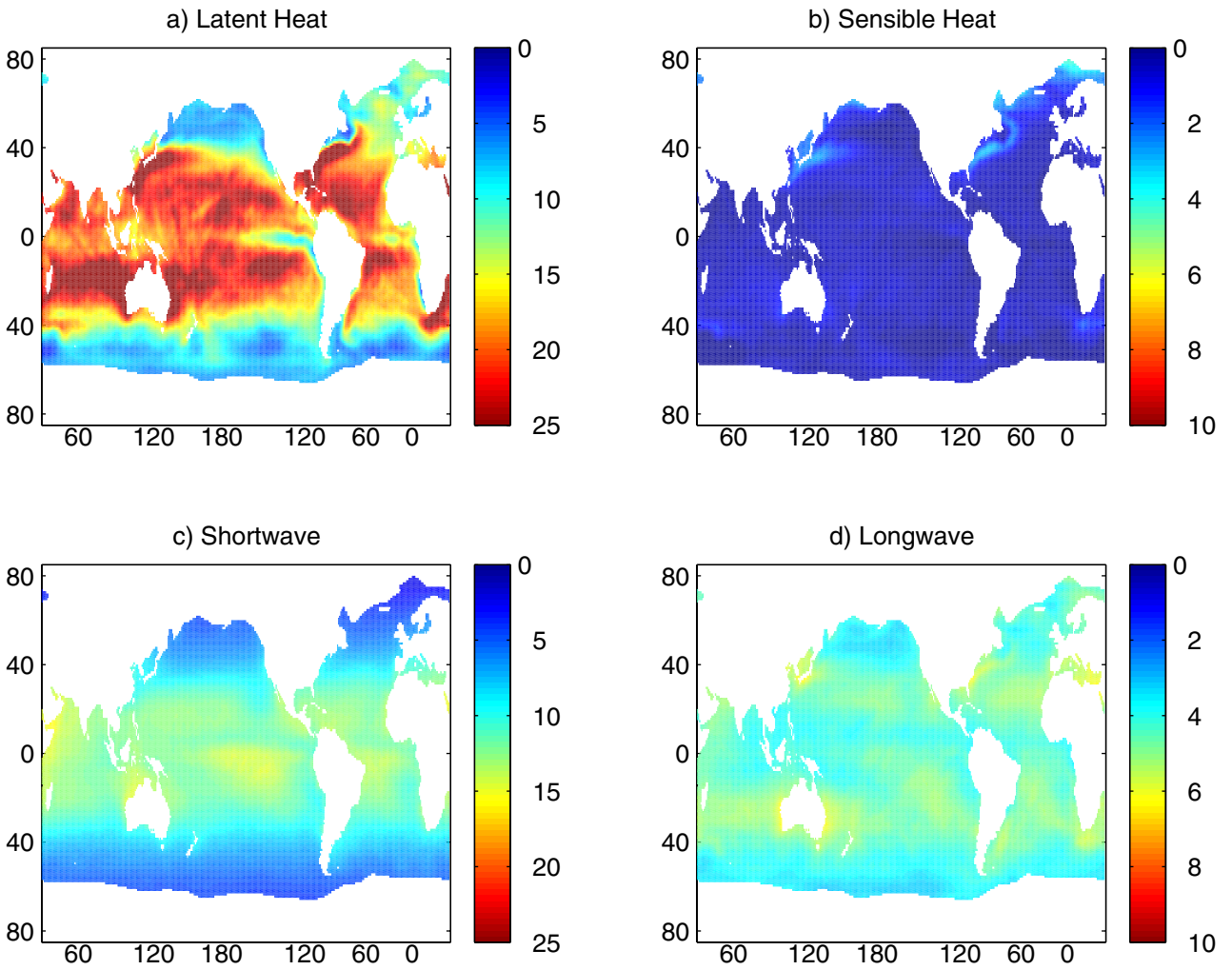


Figure 8. Maps showing the difference (adjusted -original) between the adjusted and original SOC heat flux components for Solution E (units W/m<sup>2</sup>). Note that panels a) and c) have a different scale to b) and d).

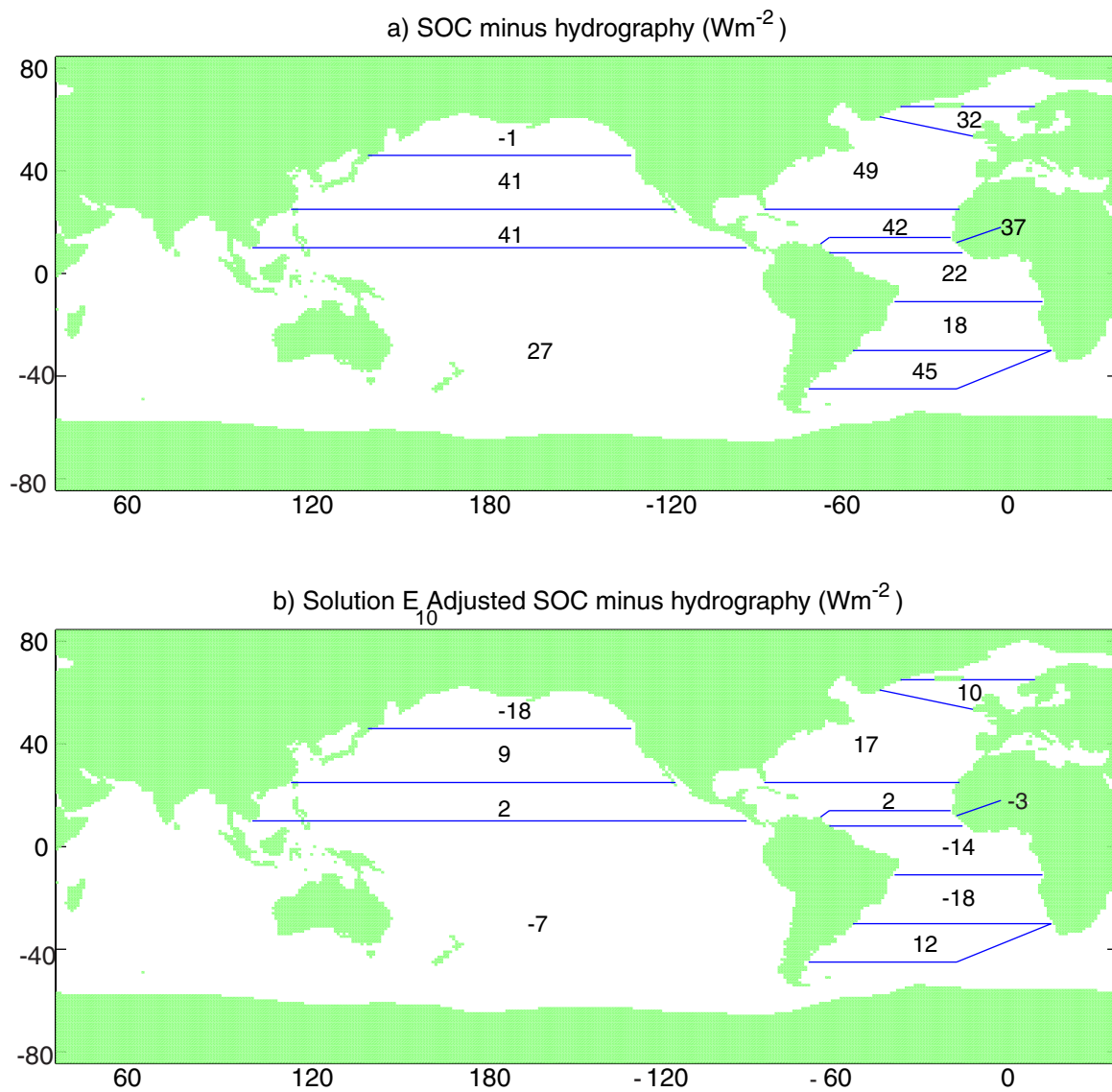


Figure 9. Schematic representation of the differences (SOC-hydrography) in the area averaged heat flux from the SOC climatology and that implied by hydrography for a) the original SOC climatology and b) the SOC climatology adjusted according to solution  $E_{10}$  (units  $W/m^2$ ).

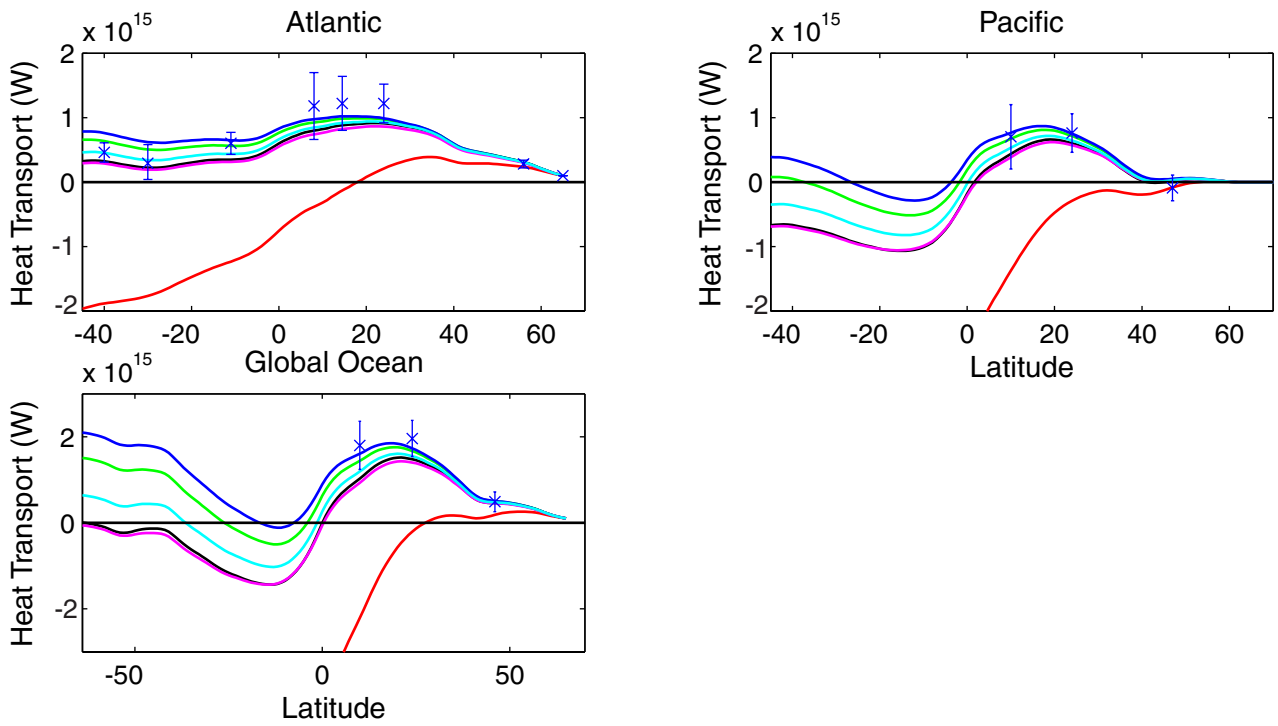


Figure 10. Climatologically implied ocean heat transport for a) the Atlantic Ocean, b) the Pacific Ocean and c) the Global Ocean for the original SOC climatology (red line), solution  $A_{10}$  (green), solution  $B_{10}$  (blue), solution  $C_{10}$  (black), solution  $D_{10}$  (magenta) and solution  $E_{10}$  (cyan). Blue crosses indicate hydrographic estimates of the heat transport.

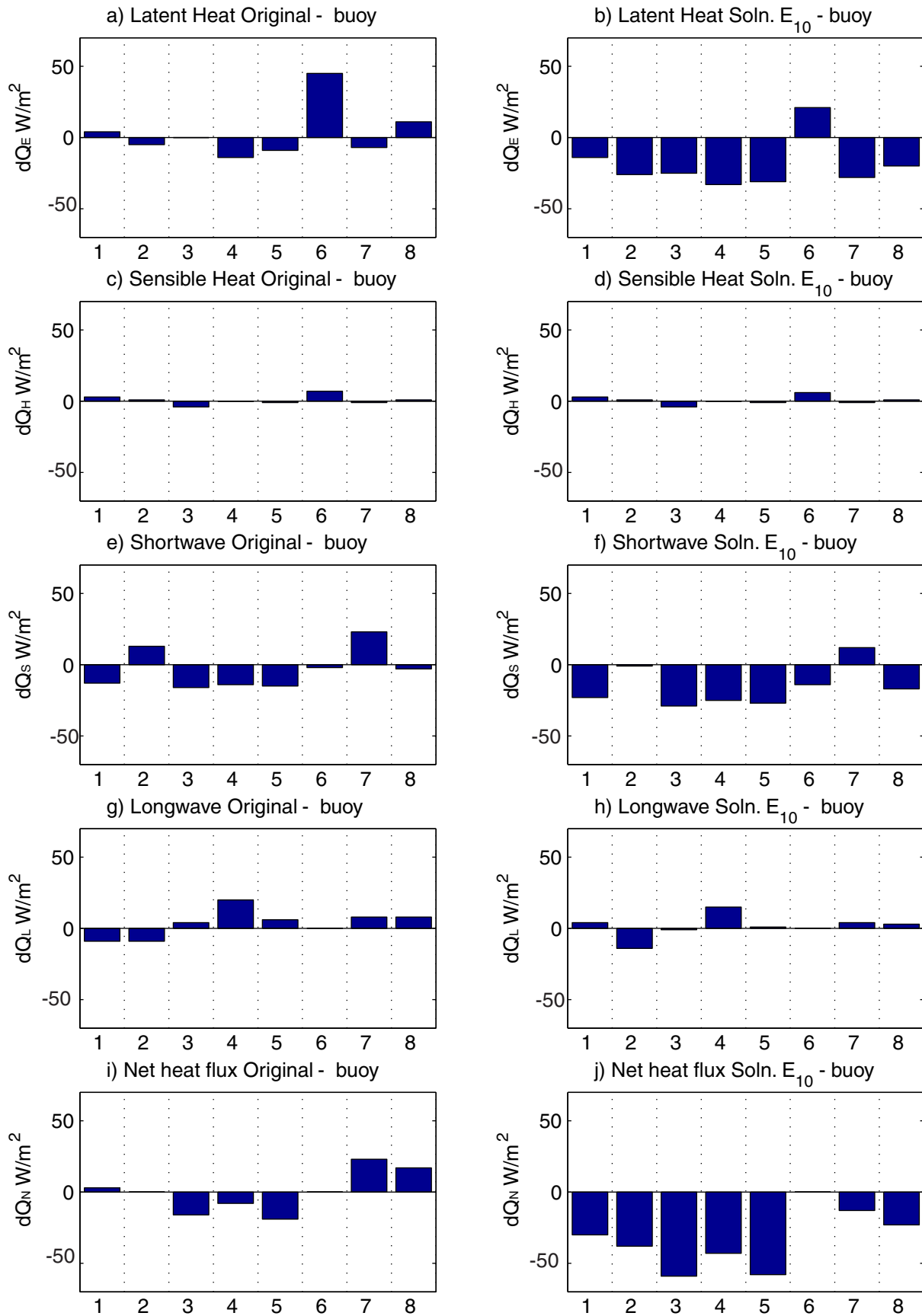


Figure 11. Summary plot showing the difference between the SOC estimates and WHOI research buoy measurements of the various heat flux components and the net heat flux. Left hand column : differences between the original SOC climatology and the buoys. Right hand column : differences between adjusted SOC Solution E10 and the buoys. The numbers refer to the different buoys considered as follows: 1 - NE buoy (subduction array); 2 - SE buoy (subduction array); 3 - SW buoy (subduction array); 4 - NW buoy (subduction array); 5 - Central buoy (subduction array); 6 - FASINEX buoy; 7 - TOGA buoy; 8 - Arabian Sea Buoy. Note that buoy measurements of the longwave and net heat flux were not available for FASINEX.